Modelling fluidized dense phase conveying of Geldart A powders with MFiX-TFM: A case study

Prabu Balasubramanian, Andrew Cowell, Don McGlinchey

School of Computing, Engineering and Built Environment
Glasgow Caledonian University, United Kingdom

Outline

- Fluidized Dense Phase Conveying
  - Typical system and operating conditions
  - On Vertical phase map
  - On Horizontal phase map
- Characteristics of the Geldart A powder
  - Powder selection and characteristics
  - Recent CFB experiments – HD-CFB or LD-CFB?
- Modelling options
  - Model scheme
  - Drag model
  - Wall BC
  - Coordinate systems
  - Cloud computing
  - Parallel processing
- Numerical modelling intricacies
  - Numerical artifacts
  - Under-relaxation factors to prevent backflow
- Simulation results
- Conclusions

Graphical Abstract

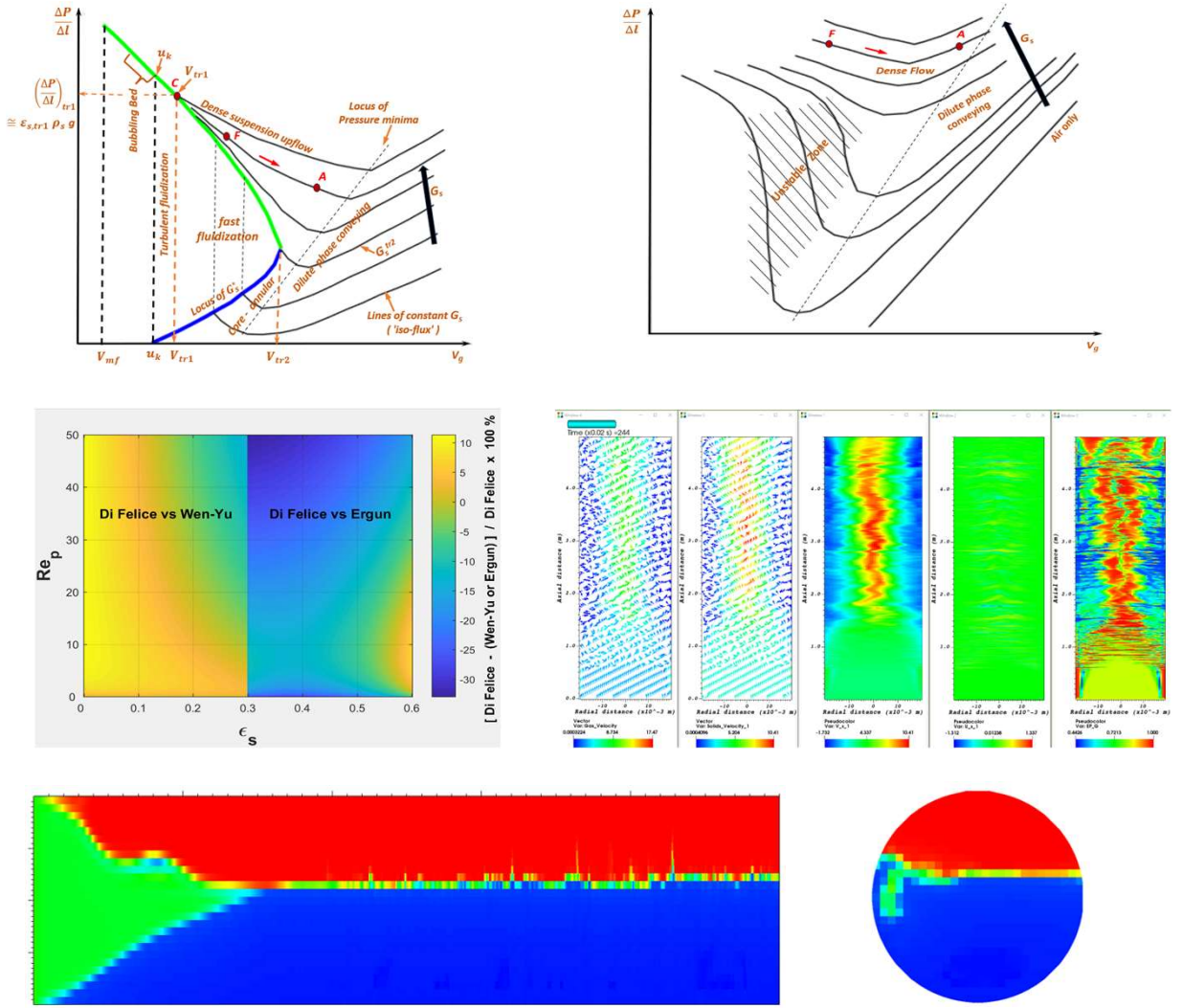

Fluidized Dense Phase Conveying

Fluidized dense phase conveying

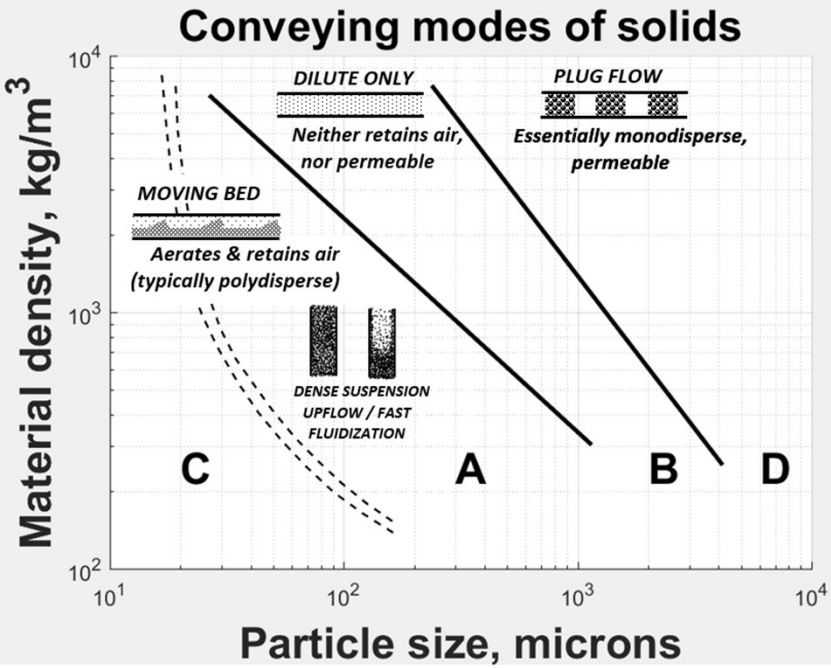

- Suitable for fine powders (Typical Geldart A or C) that aerate and retain air well.
- Design remains largely empirical, requiring full-scale experiments with the product; Eulerian modelling is an attractive alternative.

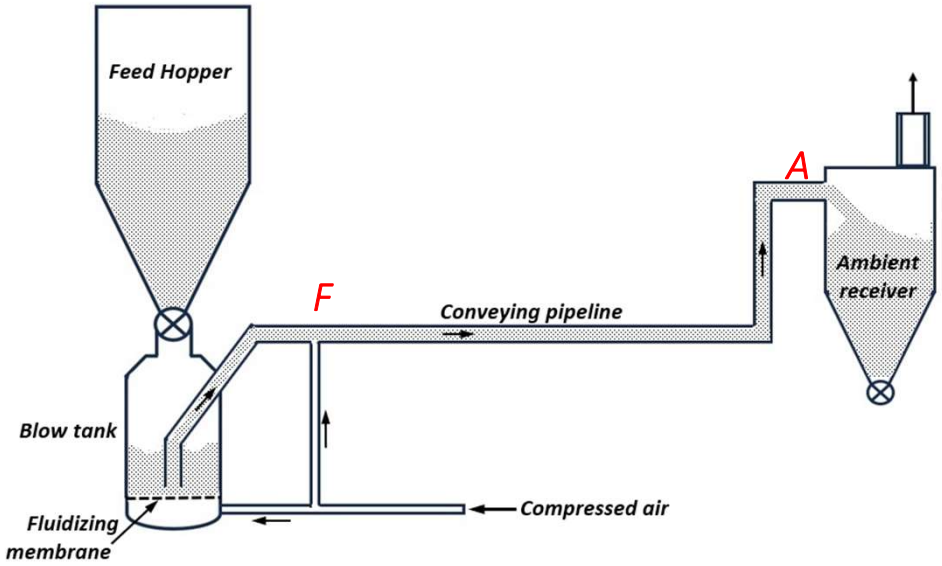

Typical Fluidized Dense Phase Conveying System and Operating Conditions Reference: Mills (2004)

Description		Feed zone (***F***)	Ambient Receiver (***A***)
Maximum Solids loading (m)	kg / kg of air	150 - 300	
Maximum Solids flux (G_s)	kg / m^2 s	1000 - 3000	
Pressure	bar	2.5 - 4.0	Ambient
Solids volume fraction (ε_s)	-	0.12 - 0.30 *	0.04 - 0.14
Superficial gas velocity (V_g)	m / s	3 - 4	9 - 12
Conveying Pipeline	-	Typically, up to a few hundred meters long, > 80 % horizontal, with several bends	

* - For powders that show clear pressure minima in the phase diagram.

Fluidized Dense Phase Conveying on Vertical Flow Phase Map

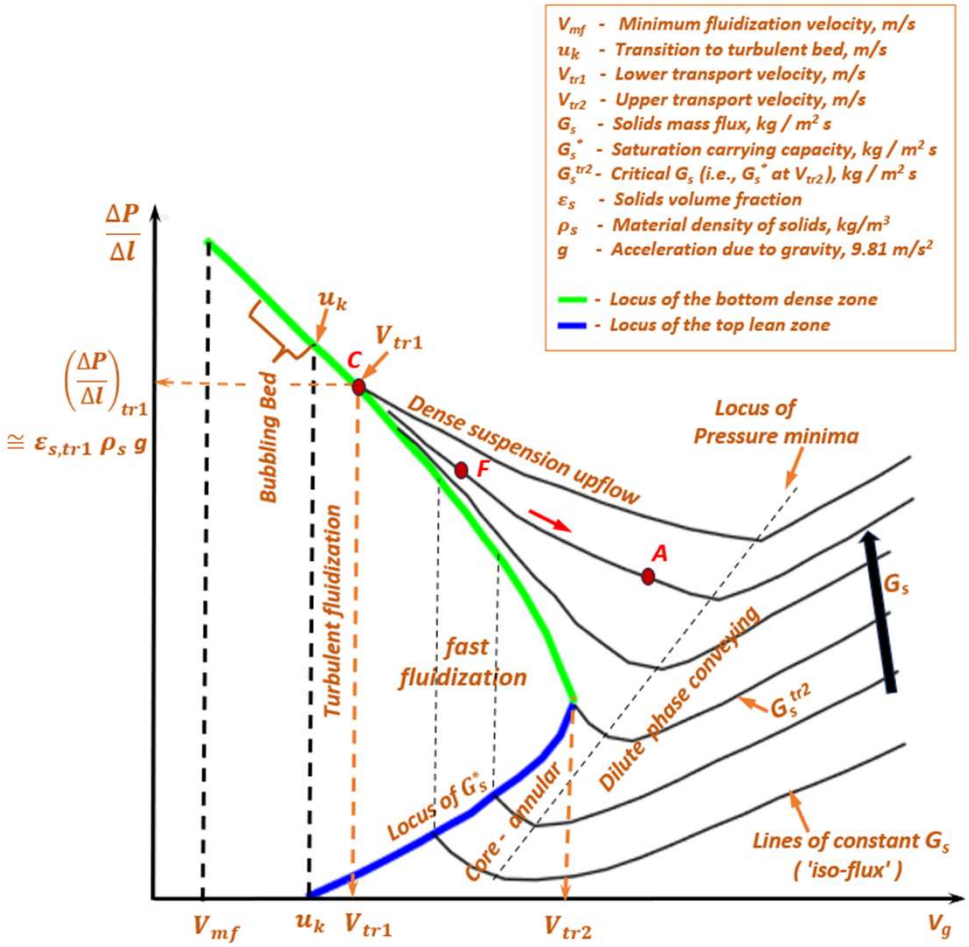

Vertical flow: Phase map of Wirth adapted for Geldart A powders

Reference: Adapted from Wirth (1988), with inputs from Yerushalmi & Avidan (1985), Kim et al. (2004), Cocco et al. (2010), Monazam & Shadle (2011), Breault (2023)

- Experimental data (Mills, 2004) suggests that, at high G_s the flow occurs at dense conditions (e.g., *F* → *A*) wherein 'bed filling' is irrelevant; flow may not transition to dilute phase conveying ($\varepsilon_s < 0.02$) at the ambient receiver.

  (*Note: It is assumed here that the change in operating pressure does not affect the phase map.*)
- Dense Suspension Upflow (DSU) is also broadly 'core-annular flow', with denser annulus and relatively dilute core, but with up flowing annulus. However, axial variation in ε_s is limited to the expansion of air for the incurred pressure drop.
- As DSU operates at higher ε_s than fast fluidization (0.07-0.25 against 0.03-0.10) for the same range of V_g, slip velocities are even higher (3-10 m/s against 2-6 m/s) Grace(2000).
- At lower G_s, the locus of G_s^* marks the 'onset of accumulative choking'. Axial variation in ε_s follows the 'S-shaped profile' with a Transport Disengagement Height (TDH) between the dense and lean zones. The operation (solids inventory) can be very sensitive to variations in G_s and/or V_g (Monazam & Shadle (2011)) ; however, it is a well-established operating regime in industry.

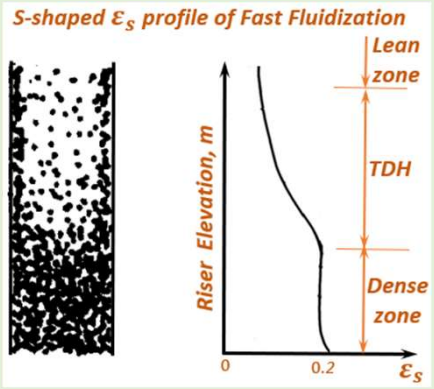

Reference: Kunii & Levenspiel (1991)

- For all cases choking is complete at *C* (V_{tr1} , $\varepsilon_{s,tr1}$), wherein net entrainment has essentially stopped, and the solids have collapsed into a turbulent bed.

Fluidized Dense Phase Conveying on Horizontal flow Phase Map

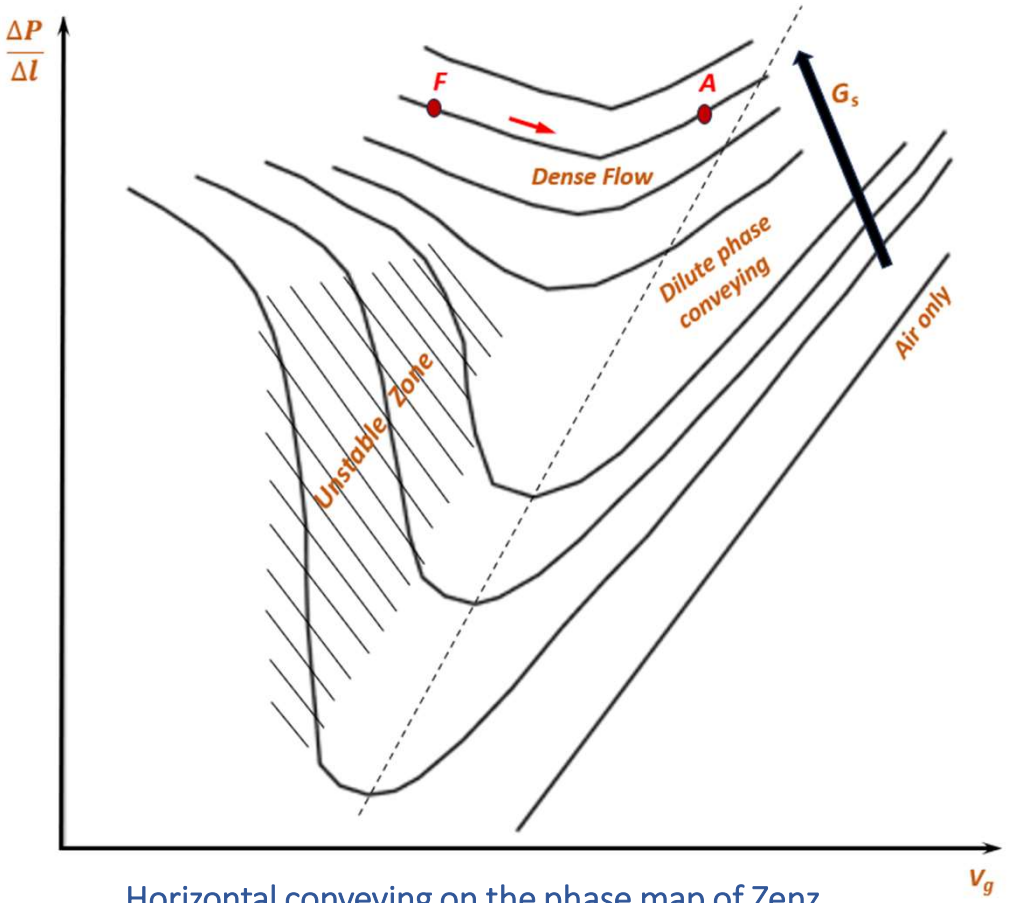

Horizontal conveying on the phase map of Zenz

Reference: Adapted from Zenz(1949) for fine powders, with inputs from Mills (2005), Canning & Thompson (1982) cited in Klinzing et al. (2010).

- Experimental data (Mills (2004), Canning & Thompson (1982) (cited in Klinzing et al. (2010)) suggests that, at high solids loading (1000 – 3000 kg/m^{2}s) flow occurs at dense conditions (e.g., *F* → *A*) where 'saltation' (unstable zone) is irrelevant.
- Experimental data (Mills, 2004) also indicates that dense flow at higher G_s occurs on either side of the pressure minima (intuitive as there is no static head of solids).
- Typical 'moving bed' dense horizontal flow pattern:

Reference: Klinzing et al. (2010)

Dilute phase conveying (ε_s < 0.02) may coexist at the top of the pipe cross section with a moving dense bed of solids (ε_s up to 0.6) at the bottom.

- Given the very high G_s it may not be practical to pick up and accelerate solids fed to rest at the bottom of the pipe; instead, the solids are fed fluidized from the blow tank.

Characteristics of the Geldart A powder

Selection and Characteristics of the (hypothetical) powder

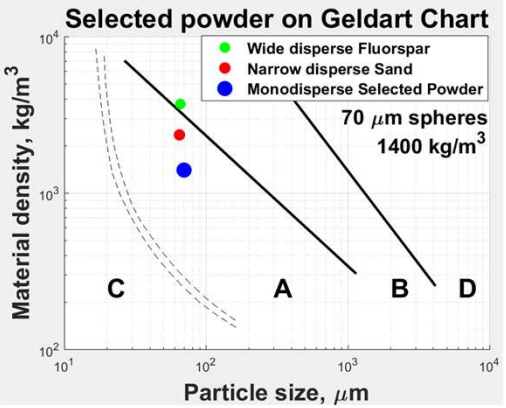

For smaller d_p

- Ability of a powder to aerate and retain aeration is critical for fluidized dense phase conveying.
- Powders at the Geldart A-B boundary, may show interchanged flow behaviour depending on their ability to retain air, i.e., the width of size distribution.
- For a monodisperse Geldart A powder to flow by fluidized dense phase, it should be away from A-B boundary (low in ρ_s and d_p).

Note: Geldart chart is based on ambient air. At higher pressures (such as at F), Geldart A/B boundary may shift to the right (i.e., to higher mean particle size) (Yang (2007)).

Against smaller d_p

- Cohesion due to van der Waals forces become significant at $d_p < \sim 55$ μm (Wang et al.(2011), Loezos et al. (2002)). Cohesion models are not available in standard MFiX-TFM.

  (*Askarishahi et al.(2022) have reported a custom implementation of the cohesion model of Gu et al.(2019) in MFiX*)
- Computationally prohibitive, as cells of ~10 d_p is required for reliable predictions and ~20 d_p for even reliable qualitative trends (Agrawal et al.(2001), Benyahia et al.(2007)).

Characteristics of the selected powder at ambient conditions

Archimedes number	***Ar***		**17.5**	
Void fraction loose packed	$\varepsilon_{s,max}$		**0.60**	Maximum packing limit
Interparticle restitution	***c_e***		**0.87**	Foerster et al. (1994), Drake (1991), (6 mm cellulose acetate spheres) (Note-1)
Particle – wall restitution	***e_w***		**0.89**	
Angle of wall friction	***Phi_w***	°	**11.86**	
Angle of internal friction	***Phi***	°	**30**	McKeen & Pugsley (2003)
Terminal settling velocity	V_t	m / s	**0.186**	
Min. fluidization velocity	V_{mf}	m / s	**0.004**	Kunii & Levenspiel (1991)
Min. bubbling velocity	V_{mb}	m / s	**0.012**	
Lower transport velocity	V_{tr1}	m / s	**1.95**	Yerushalmi & Avidan (1982) ('HFZ-20 catalyst', 49 μm, 1450 kg/m³, D_r = 152 mm) (Note-2)
Upper transport velocity	V_{tr2}	m / s	**> 5.20**	
Critical G_s (i.e., G_s^* at V_{tr2})	G_s^{tr2}	kg / m² s	**> 236**	Breault & Weber (2021)

Particles are non-cohesive, do not agglomerate or deform permanently, and there are no electrostatic effects.

An important criterion in the selection of powder is the availability of experimental data for model validation. The selected particle size and material density corresponds to FCC particles for which experimental data is widely reported (although all for vertical flow). However, one-to-one correspondence cannot be expected between the model which considers a monodisperse powder and experiments with polydisperse powders that contain a significant fraction of fines (dp < 44 μm).

Note-1: Restitution coefficients of 0.90 – 0.95 is widely used in the literature. Indicated values may be revised higher during model validation to match experimental radial profiles for solids fraction.

Note-2: The correlations available in the literature (such as Bi & Grace (1995) and Monazam & Shadle (2011)) underpredict V_{tr1} and V_{tr2} for fine powders.

Indicated V_{tr2} of 5.2 m/s from Yerushalmi & Avidan (1982) corresponds to the transition to 'Dense Conveying' (i.e., core-annular flow) at a G_s of 150 kg/m²s .

!? *Ar* based correlations (e.g., V_{tr1} , V_{tr2} , G_s^*) are largely based on data at essentially atmospheric pressure. As $Ar\ (= \rho_g\,(\rho_s - \rho_g)\,g\,d_p^3 / \mu_g^2)$ scales with pressure (i.e., ρ_g), it is not clear from the literature if the correlations are suitable for pressures higher than atmospheric, such as at the feed zone, *F*. !?

Recent CFB experiments – HD-CFB or LD-CFB ?

- Issangya et al. (2022) have recently reported S-shaped ε_s profile at as high as G_s as 636 kg/m²s and V_g of 9 – 16 m/s, with a riser diameter (D_r) of 0.3 m. They have observed dense suspension at the bottom of the riser to coexist with dilute phase conveying at the top.
- Dense suspension upflow requires both $V_g > V_{tr2}$ and $G_s > G_s^{tr2}$.
- Wang et al.(2022) have observed the S-shaped ε_s profile disappear only at a $G_s \sim 1000$ kg/m²s and $V_g \sim 9$ m/s, for a D_r of 0.08 m.
- As it can be seen in the correlation of Breault & Weber (2021), G_s^{tr2} scales directly with the riser diameter, D_r. (This correlation is based predominantly on FCC particles and covers data over $5 < Ar < 20.1$, $0.066 < D_r < 0.15$ m, $1.09 < V_g < 4.00$ m/s, $2.31 < G_s^* < 198$ kg/m²s.)

$$G_S^* = 318 \frac{D_r V_g^{(0.000716\, d_p^2)}}{Ar}$$

- Results of Wang et al.(2022) and the estimates for G_s^{tr2} based on Breault & Weber (2021) (extrapolated beyond the data range of the correlation) suggest that the maximum G_s of 636 kg/m²s used in the experiment was most probably below G_s^{tr2}.

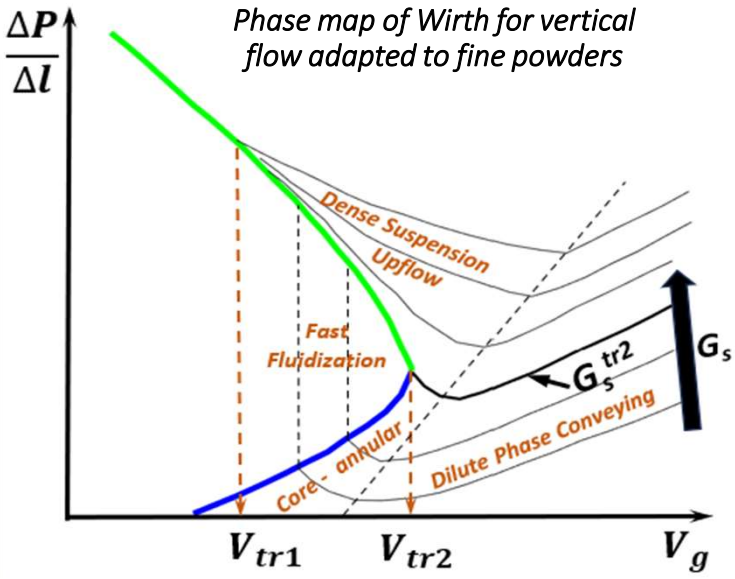

Phase map of Wirth for vertical flow adapted to fine powders

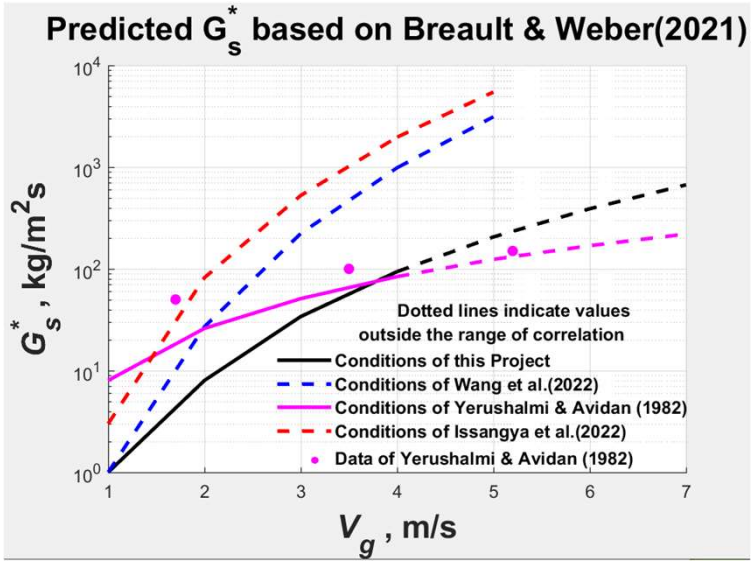

Conditions of the experiments

Description	This Project	Wang et al. (2022)	Yerushalmi & Avidan (1982)	Issangya et al. (2022)
Riser diameter (D_r) , m	0.04	0.08	0.152	0.303
Riser height, m	--	18.0	8.5	20.4
Mean particle size (d_p), µm	70	85	49	80
Material density (ρ_s), kg/m³	1400	1500	1450	1490
Archimedes number *(Ar)* (ambient)	17.5	33.6	6.2	27.8

Modelling Options

Model scheme

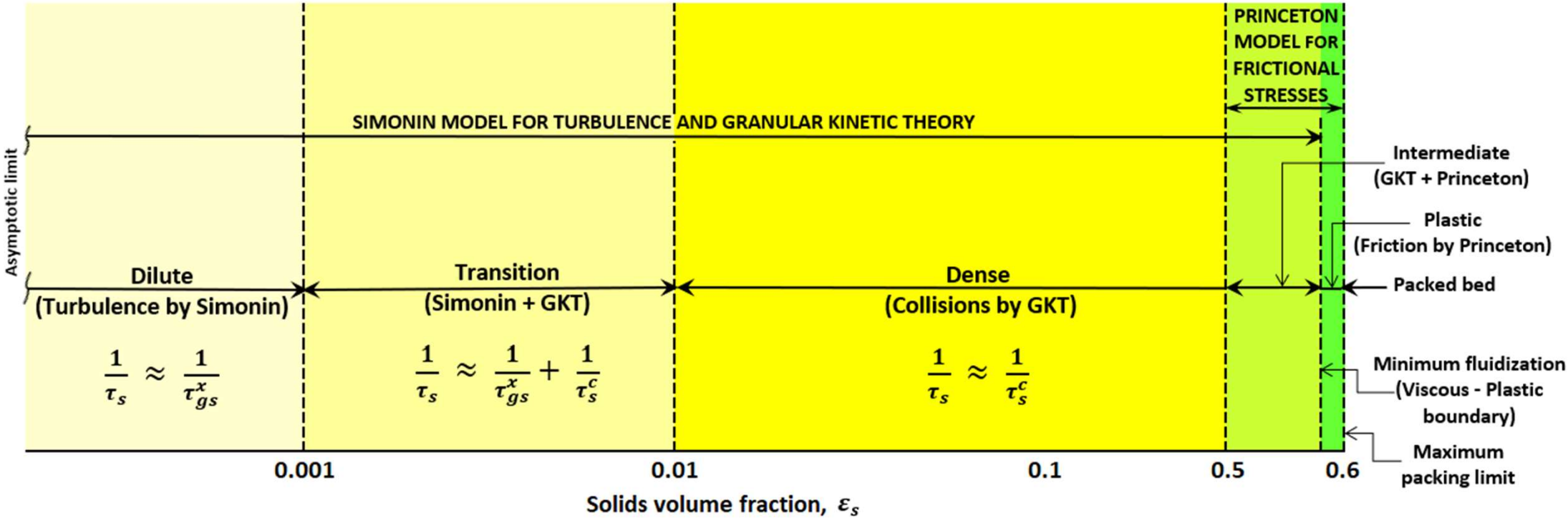

Simonin viscous stress model covers dilute turbulent through to the dense limit of viscous regime by a harmonic mean of collisional and particle relaxation time scales; Simonin's turbulence model and the GKT are recovered at the dilute and dense limits, respectively.

τ_s - Dissipation time scale, s **τ_{gs}^x - Particle relaxation time, s** **τ_s^c - Collisional time scale, s**

Reference: Balzer et al.(1996) Benyahia et al.(2005) & (2007), Srivastava & Sundaresan (2003)

Selection of drag model

Type	Model	Applicable Range
Empirical	**Gidaspow blend** (Lathouwers & Bellan (2000)) (Smooth transition between Wen-Yu and Ergun at ε_s = 0.2)	$0 \le \varepsilon_s \le 0.6$ $0.01 \le Re_p \le 5000$
	Syamlal – O'Brien (1987)	$0 \le \varepsilon_s \le 0.6$ $0.1 \le Re_p \le 10000$
	Di Felice (1994) (Based on Dalla Valle isolated sphere correlation)	$0 \le \varepsilon_s \le 0.6$ $0.01 \le Re_p \le 10000$
DNS	**Koch-Hill-Ladd** (2001)	$0 \le \varepsilon_s \le 0.6$ $0 < Re_p < 120$
	Beetstra et al. (2007)	$0 \le \varepsilon_s \le 0.6$ $0 \le Re_p \le 1000$
	Tang et al. (2015)	$0 \le \varepsilon_s \le 0.6$ $0 \le Re_p \le 1000$
	Tenneti et al. (2011) (Hybrid with Schiller & Naumann isolated sphere correlation)	$0 \le \varepsilon_s \le 0.5$ $0.01 \le Re_p \le 300$

Adapted from Leboreiro et al. (2008)

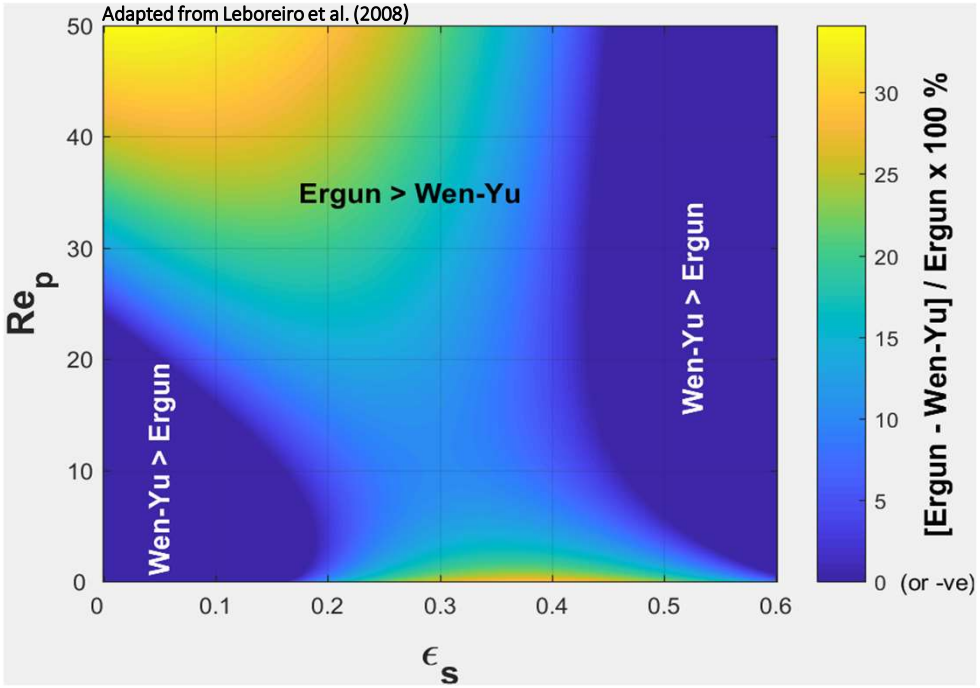

- Drag force is a function of ε_s and Re_p based on slip velocity.
- Project range: $0 < \varepsilon_s < 0.6$ and $Re_p < \sim 100$ (high slip velocities in DSU).
- For the project purpose, a homogeneous drag law is essential; heterogeneous drag laws intended for macroscale models are excluded.
- DNS drag laws overpredict at dilute conditions ($0 < \varepsilon_s < 0.2$), constrained by computing power for modelling the unbounded condition of an isolated sphere. (Tang et al. (2015))
- Tenneti et al. hybrid model does not cover the full range of ε_s
- Syamlal-O'Brien drag law is suitable for higher velocities but may not be near close packed conditions (Bakshi et al. (2015), Arastoopour et al.(2017)).

Transition in the Gidaspow blend drag model

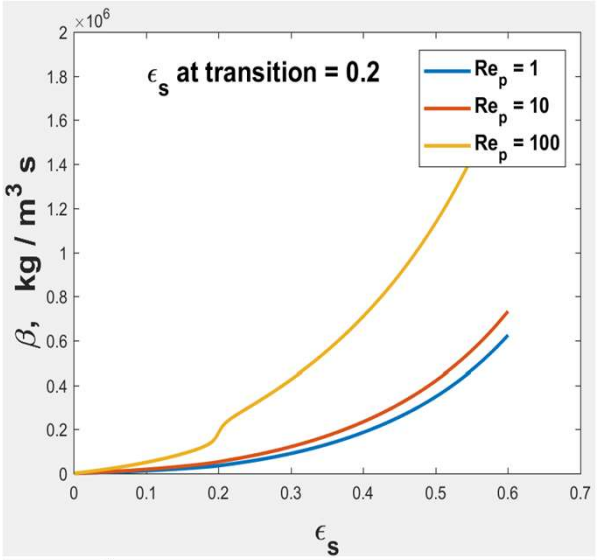

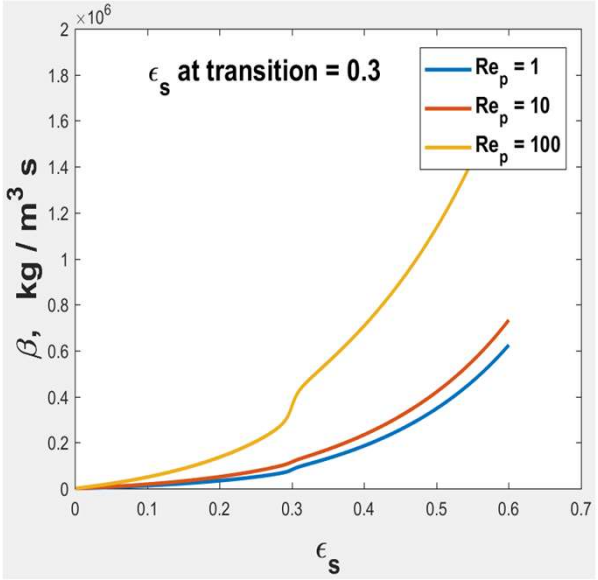

- Transition between Wen-Yu and Ergun in Gidaspow blend is smooth with an arctan function but steep except at ε_s = 0.2 and $Re_p < \sim 10$.
- Wen-Yu (based on Schiller and Naumann) better predicts at the limit of an isolated sphere. Furthermore, LBM simulations (Kandhai et al. (2003)) have shown that Wen-Yu predicts well up to ε_s = 0.3, and that Ergun overpredicts at $0.2 < \varepsilon_s < 0.5$.
- Gobin et al. (2003) have proposed the following transition:

$$C_D = \begin{cases} min\left(C_{D,Wen-Yu}, C_{D,Ergun}\right), if\ \varepsilon_s > 0.3 \\ C_{D,Wen-Yu}\ , if\ \varepsilon_s \le 0.3 \end{cases}$$

I.e., essentially at the Wen-Yu = Ergun boundary on the right side, at ε_s > 0.4. However, Wen-Yu may not be suitable at ε_s > 0.3.

Di Felice drag model

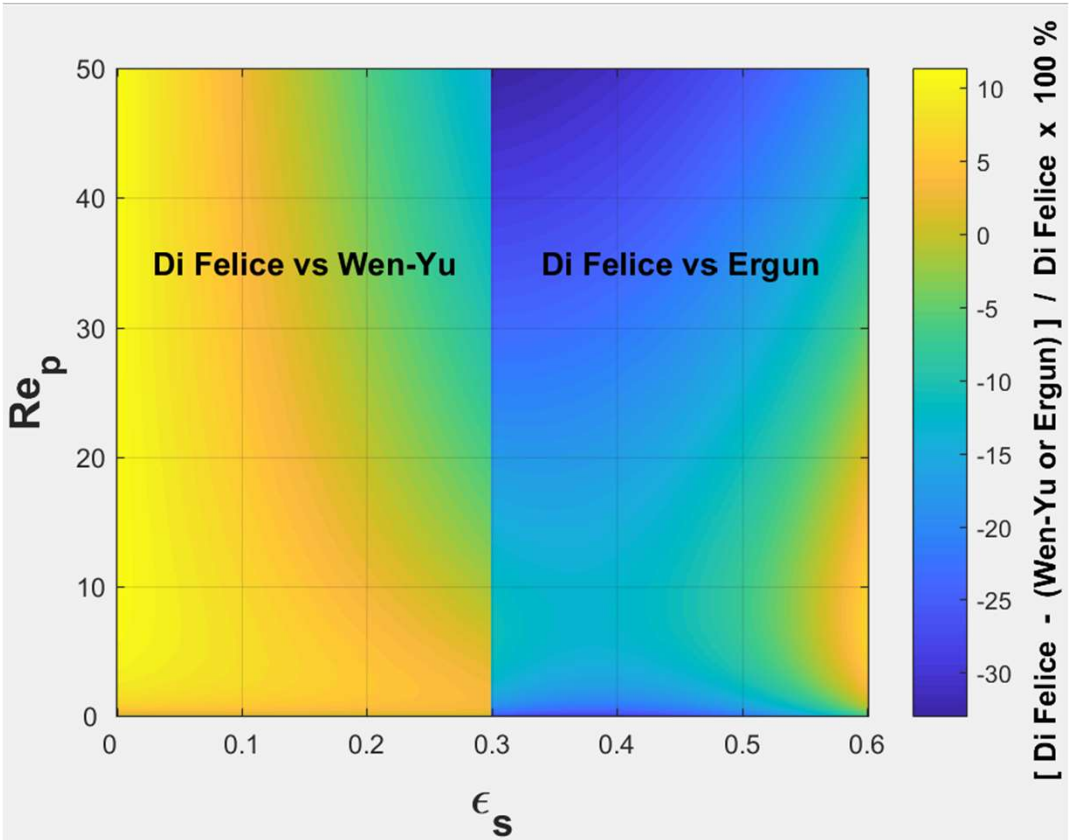

- Di Felice (1994) correlated the Ergun equation for closely packed conditions together with experimental data for dilute and intermediate ε_s .
- A correction is applied to the Dalla Valle isolated sphere correlation in terms of void fraction, with an empirical exponent; the exponent is a (weak) function of Re_p .

$$\beta = \frac{3}{4} C_D \frac{\varepsilon_s \varepsilon_g \rho_g \left|\vec{u}_g - \vec{u}_s\right|}{d_p} \varepsilon_g^{\left(-2.7+0.65\, exp\left\{\frac{-(1.5-\log_{10} Re_p)^2}{2}\right\}\right)}$$

$$C_D = \left(0.63 + {}^{4.8}/_{\sqrt{Re_p}}\right)^2$$

- Di Felice model predicts within 10 % of Wen-Yu at ε_s < 0.3 and also within 10 % of Ergun at 0.5 < ε_s < 0.6 for the expected project range of Re_p ; underpredicts Ergun by up to 20% at 0.3 < ε_s < 0.5 for the expected project range of Re_p (which may be desirable too, as Ergun is reported to overpredict in this range).
- The model is continuous over the full range of ε_s .

Note: As the Di Felice exponent was correlated using the Dalla Valle isolated sphere correlation, the model better conforms with Wen-Yu and Ergun at the applicable ranges of ε_s with the Dalla Valle correlation than with the Schiller & Naumann correlation.

Amongst other interfacial forces (virtual mass, history, spin lift and slip-shear lift), the slip-shear lift force can be notable due to strong gradients in gas velocity, especially for horizontal flow (Massoudi(2003), Patro & Dash (2014)). However, it is not available in the standard MFiX-TFM.

Coordinate system and Wall BC options

Coordinate system options

Description	3D cylindrical	3D Cartesian cut-cell	2D Cartesian
Sectional views	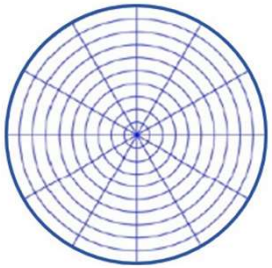 Radial section	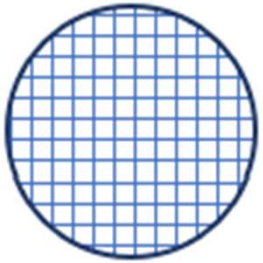 Radial section	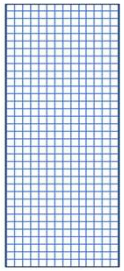 Axial section
Geometry	Exactly matches the pipe wall profile	Cartesian grid with peripheral cells cut to exactly match the pipe wall profile	Matches the wall profile in 2D
Wall BC for the solids phase	Johnson & Jackson partial slip BC, with Li & Benyahia variable specularity coefficient	Free slip (Johnson & Jackson BC is not available in standard MFiX-TFM)	Johnson & Jackson partial slip, with Li & Benyahia variable specularity coefficient
Advantages	Exactly matches with the wall profile and offers rigorous wall BC	Simplicity of Cartesian grid, without stairstep boundary at curved walls. Complex geometries can be modelled. Second order accurate in space (Kirkpatrick et al. (2003))	Qualitatively well predicts bed expansion, bubble rise, core-annular flow, clusters and streamers, etc. Lower computational cost for long pipe models (e.g., S-shaped profile). Offers rigorous wall BC.
Disadvantages	Axial BC, modelled as free slip wall with no normal flow through it, interferes with profile of gas bubbles and results in the overprediction of ε_s near the axis (Bakshi et al. (2014) & (2015)) High resolution grids result in very small cells near the axis	Does not offer a rigorous wall BC. Some cut cells (small size or high aspect ratio) may result in inaccuracies.	Not suitable for horizontal flow given variations in azimuthal direction too. Does not capture the inherent 3D nature of gas-solids flow. Numerical predictions can be affected by asymmetric flows, e.g., inlet and outlet configurations. (Li et al. 2014-I) May not simultaneously predict axial pressure profile and radial voidage accurately. (Li et al. 2014-II)

Wall BC options

- Johnson & Jackson (1987) partial slip wall BC, with the variable specularity coefficient of Li & Benyahia (2012) is the best option for the project conditions. (Bakshi et al.(2015))

  However, it is not available for Cartesian Cut Cell coordinates in the standard MFiX-TFM.
- Free slip wall BC for the solids phase is a good approximation, as the specularity coefficient is generally very small for the higher velocities involved. (Benyahia et al.(2007))

!! *Fede et al. (2016) have used no slip wall BC with zero granular energy flux at the wall to conform with PEPT experimental data. This study was based on a Geldart B solids (monodisperse 875 μm & 740 kg/m³) at 12 bar operating pressure. However, Geldart B solids tend towards Geldart A behaviour at high pressures (Yang, 2007). In fact, Sabatier et al. (2020) have used this wall BC to validate an upflow bubbling fluidized bed of Geldart A solids (polydisperse 73 μm & 2640 kg/m³). However, further validation studies for broader operating conditions may be required.* !!

- Cubic cells are selected as the solids distribution evolves strongly in the axial direction too (Lu et al. (2009), Benyahia (2012)), and as the flow field is turbulent.
- Some cartesian grids are inherently good (fewer small cut cells & good aspect ratios). 27x27 grid (~21 d_p) is used for first pass simulations; final confirmation runs by ~10 d_p.

Cloud computing and Parallel processing

Cloud computing

Set up the case in MFiX GUI in PC

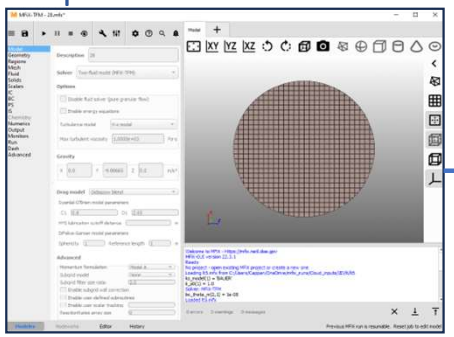

Upload .mfx

Run the case in MFiX CLI in Cloud

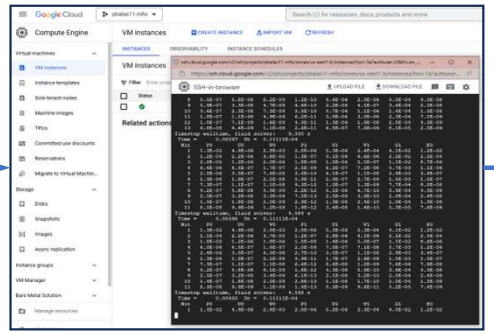

Download results

Visualize and post process in PC

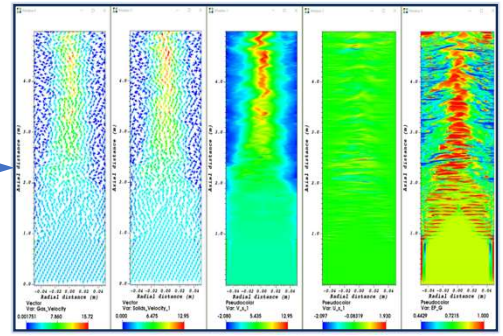

Google cloud 'Compute Optimized' C2 / C2D machines (up to 56 cores)
(MFiX 22.3.1 batch solver on Ubuntu 22.04 with GNU 11.3.0)

Parallel Processing by DMP

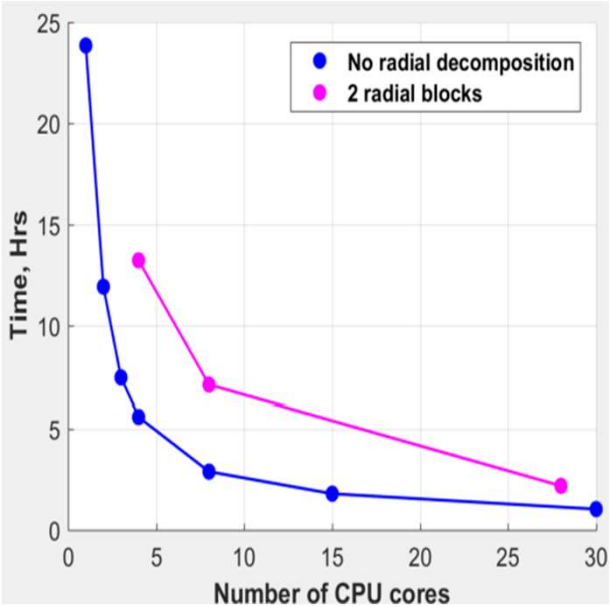

DIRECTION OF DECOMPOSITION

RUN TIMES FOR A TEST CASE SIMULATION

Google cloud C2 machines, FOUP, Preconditioner: 'NONE'

VCPU's	Physical cores	No radial decomposition		2 radial blocks		Folds increase in cores	Folds reduction in time
		Mode	Time, Hrs	Mode	Time, Hrs		
2	1	Serial	23.85			1	1
4	2	DMP-1-2-1	11.94			2	2
6	3	DMP-1-3-1	7.46			3	3
8	4	DMP-1-4-1	5.57	DMP-2-1-2	13.24	4	4
16	8	DMP-1-8-1	2.88	DMP-2-2-2	7.11	8	8
30	15	DMP-1-15-1	1.79			15	13
60	30	DMP-1-30-1	1.03	DMP-2-7-2	2.18	30	23

- For the geometry, it is optimum to decompose in the axial direction alone.
- Cases with 2 radial blocks require 4 times the cores for the same axial decomposition.
- Recommendation by Open MPI is to never specify more than the available physical cores. If 'oversubscribed', the performance is 'degraded'.
- Inter-processor communications incur a cost beyond DMP-1- 8 -1.
- Superbee took 60% longer than FOUP. Other higher order schemes were at the same ballpark.

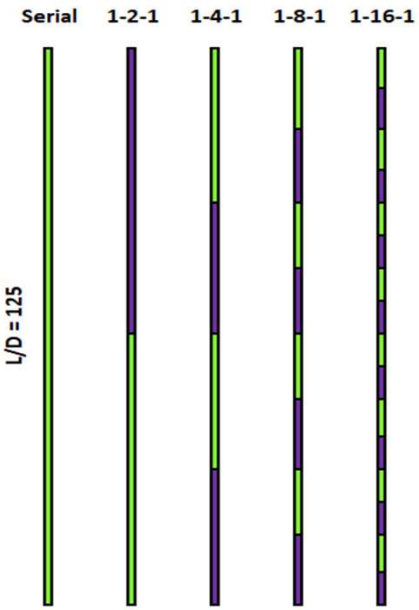

DECOMPOSITION ON GEOMETRY

Reference: MFiX user manual, Google Cloud & Open MPI web pages.

Numerical modelling intricacies

Numerical artifact: Solids accumulation at the axis with cylindrical coordinates

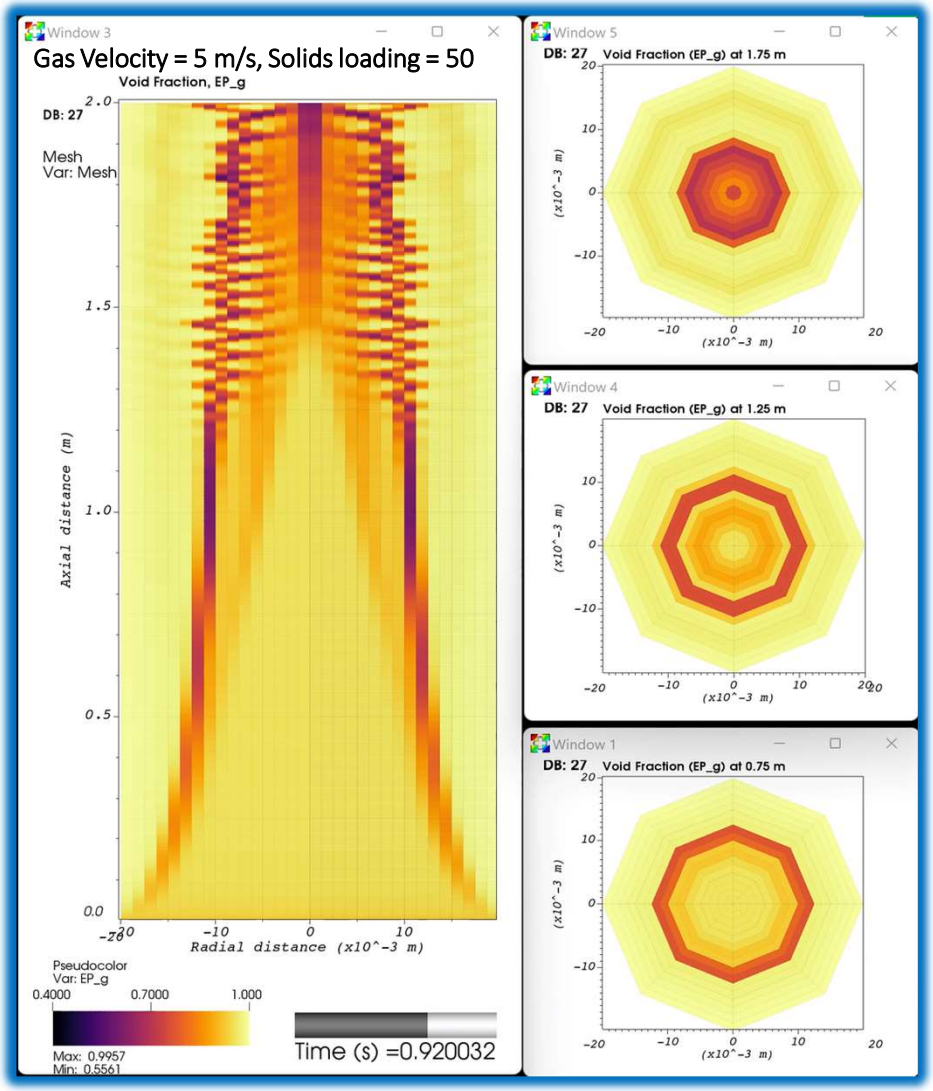

3D cylindrical, Grid: 16-512-8, diameter = 0.04 m, height = 2 m, Simonin + Srivastava, c_e = e_w =0.90, Phi_w = 8.53, BC_JJ_M, Defaults but Superbee.

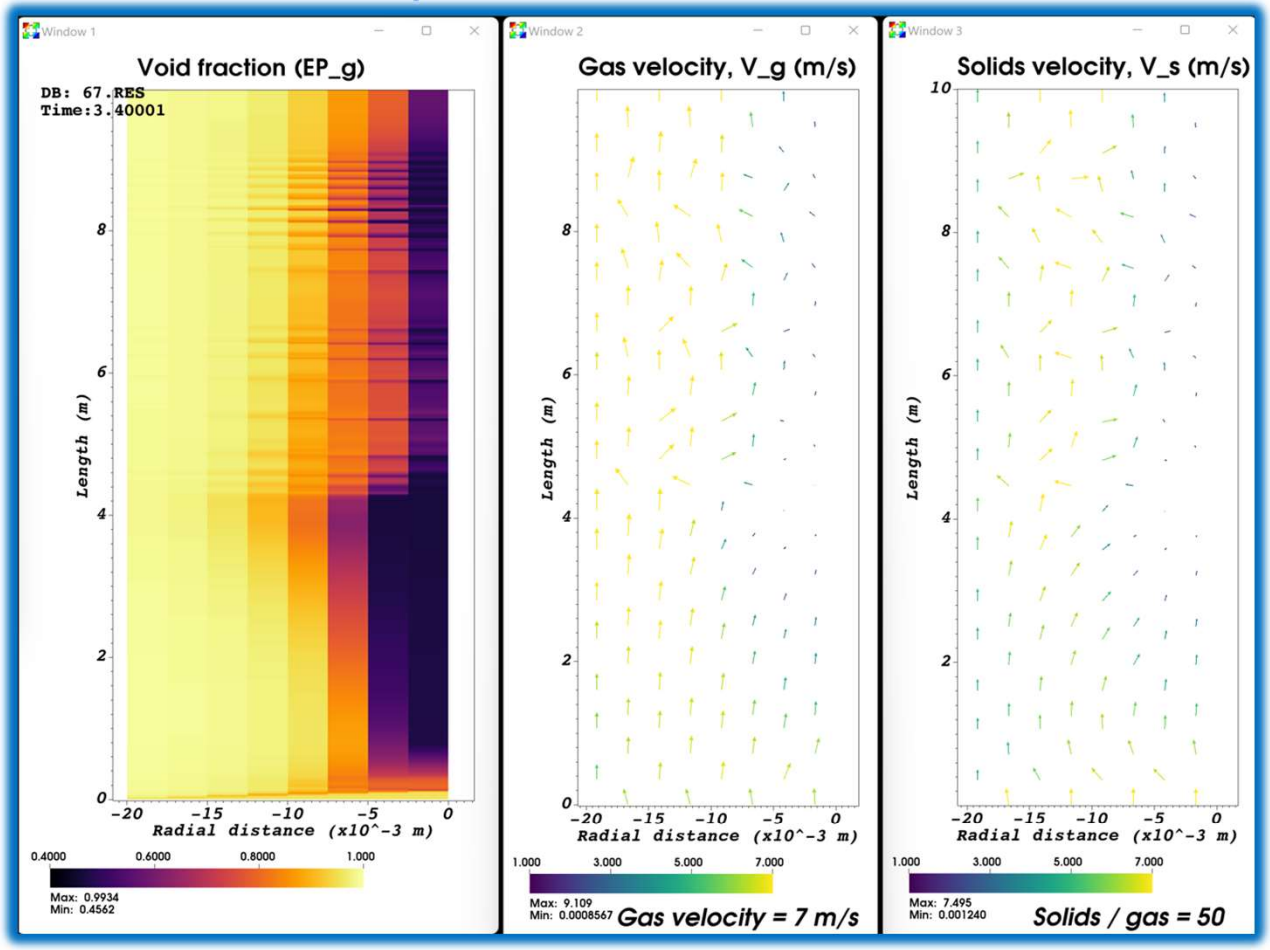

Grid: 8-2560-1, diameter = 0.04 m, height = 10 m, Simonin + Srivastava, c_e = e_w = 0.99, Phi_w = 11.31, BC_JJ_M, Defaults but Superbee.

Various parameter combinations / levels, with / without model components such as friction and turbulence, different wall BC's and IC's, etc. were tried – *In all cases solids accumulate at the axis.*

The problem with axial BC in cylindrical coordinates is documented for dense beds by Bakshi et al. (2014) & (2015). Solids accumulate at the axis modelled as a free slip wall, e.g., axisymmetric 2D simulations Li et al.(2014-II)

Numerical artifact: Solids accumulation at small cut-cells

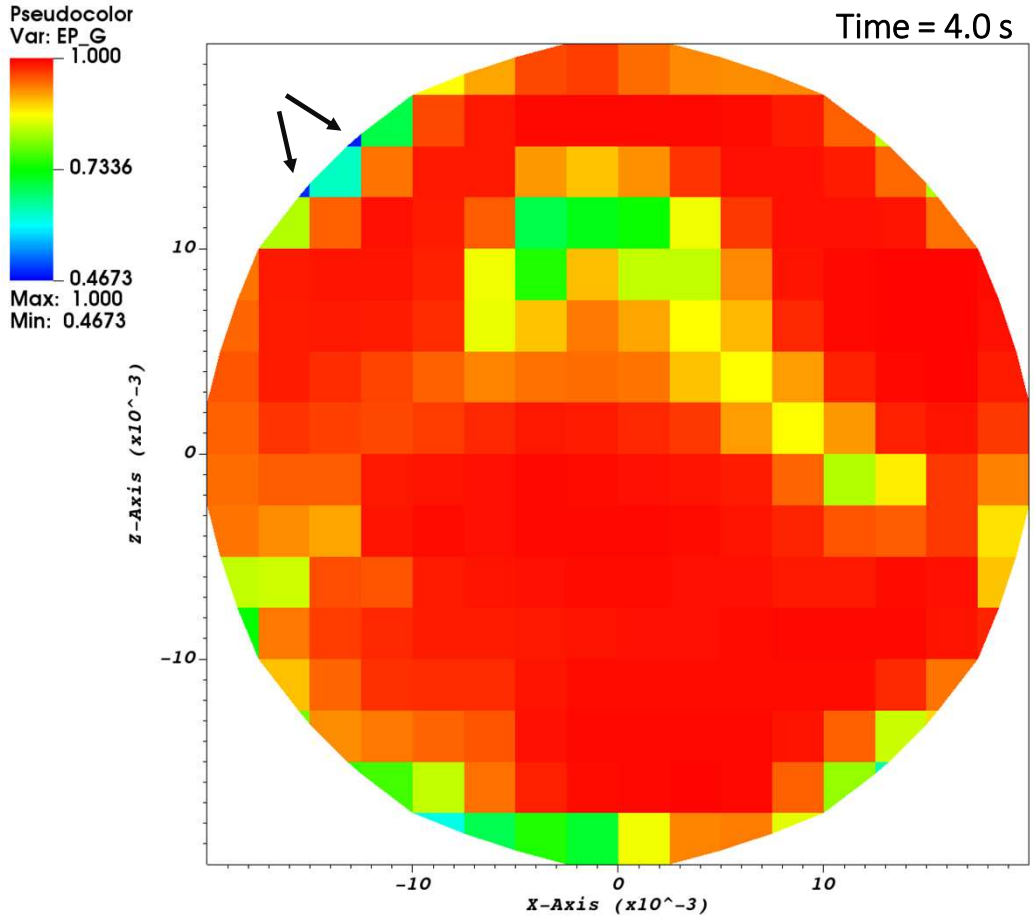

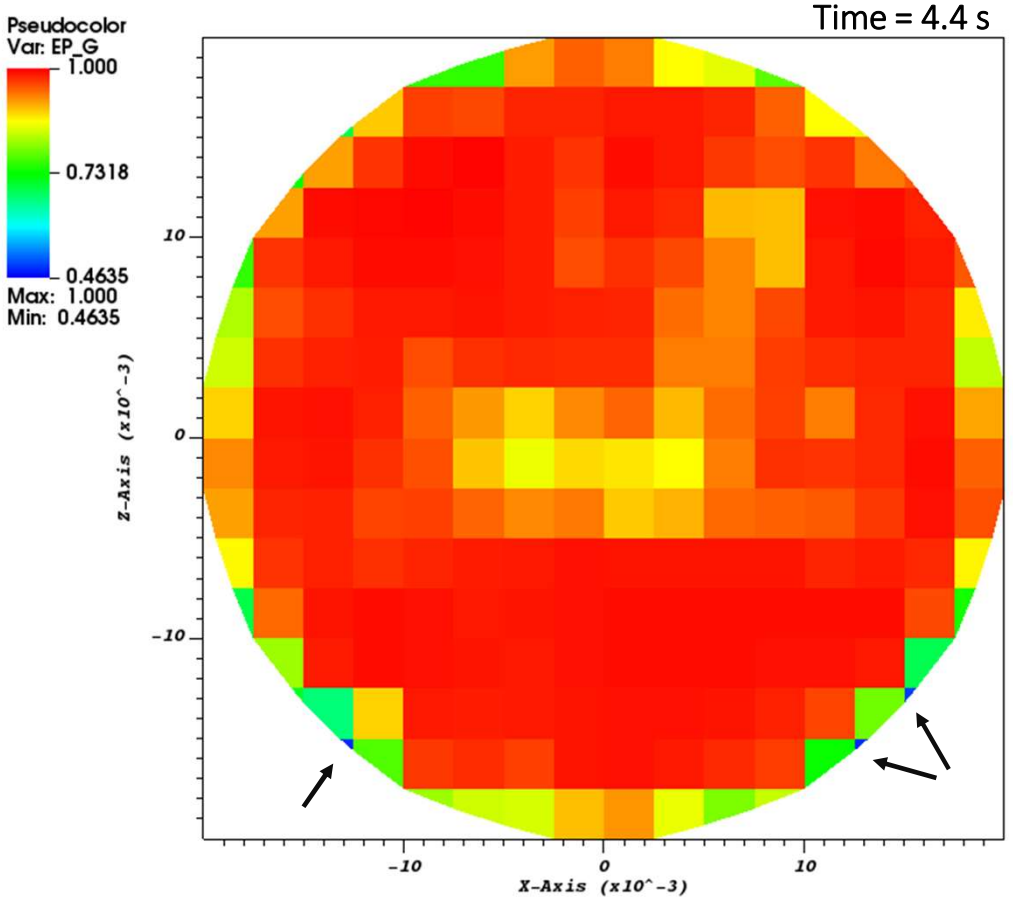

Grid: 16 x 2000 x 16, $\Delta x \sim 30\ d_p$, $\Delta t \leq$ 5.0E-5, diameter = 0.04 m, height = 5 m, Lun + Srivastava, Superbee, Gas velocity = 3 m/s, Solids loading = 50, MI-PO, Free slip wall BC, c_e = 0.99, DMP, Preconditioner: 'NONE', (Run c7)

Cross-sectional views at a height of 4.5 m

- Small cut-cells are frequently observed with higher solids concentrations than their neighbours with free slip wall BC.
- Observed with both FOUP and Superbee discretization (concentration gradient is sharp rather than diffuse).

Numerical artifact: Radial oscillations in Cartesian 2D

- Benyahia et al. (2007) have observed similar wall to wall oscillations in 1D simulations.
- Syamlal et al. (2017) have attributed this to lack of grid convergence.

Results at 5 s

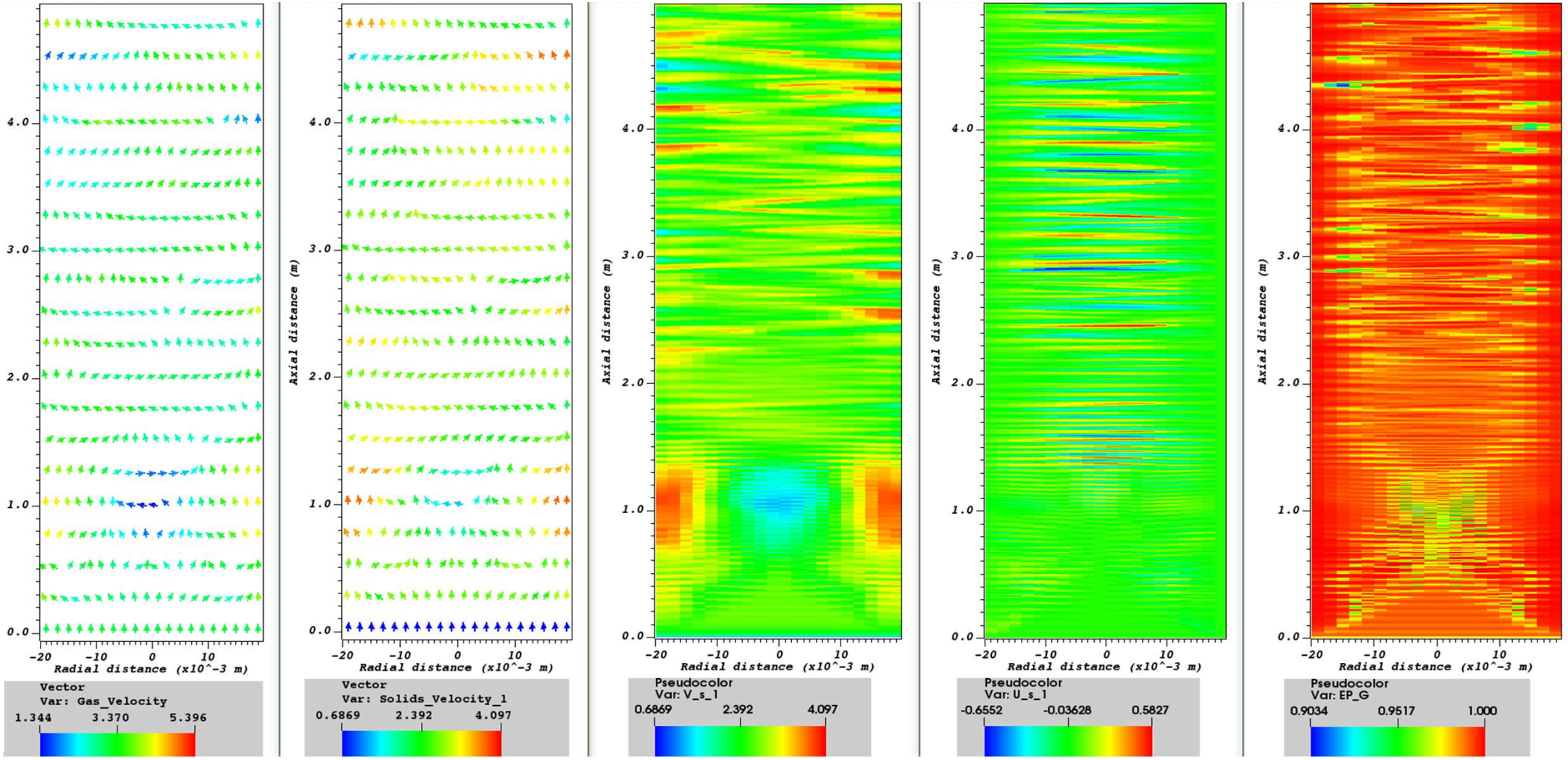

2D Cartesian, grid: 20 x 2500 x 1, $\Delta x \sim 25\, d_p$, $\Delta t \leq$ 3.0E-5, diameter = 0.04 m, height = 5 m, Simonin + Srivastava, Superbee, Gas velocity = 3 m/s, Solids loading = 10, BC_JJ_M, c_e = 0.99, e_w = 0.99, DMP, Preconditioner: 'NONE', (Run urx24r)
URFAC(1,2,4,9) = 1.0, URFAC((3&5)=0.5, URFAC(8)=0.8

Numerical artifact: Radial oscillations in Cartesian 2D

However, does not improve with finer grid (~$10d_p$) and smaller time step (1E-5). Does not respond to Numerics either.

Results at 3.9 s

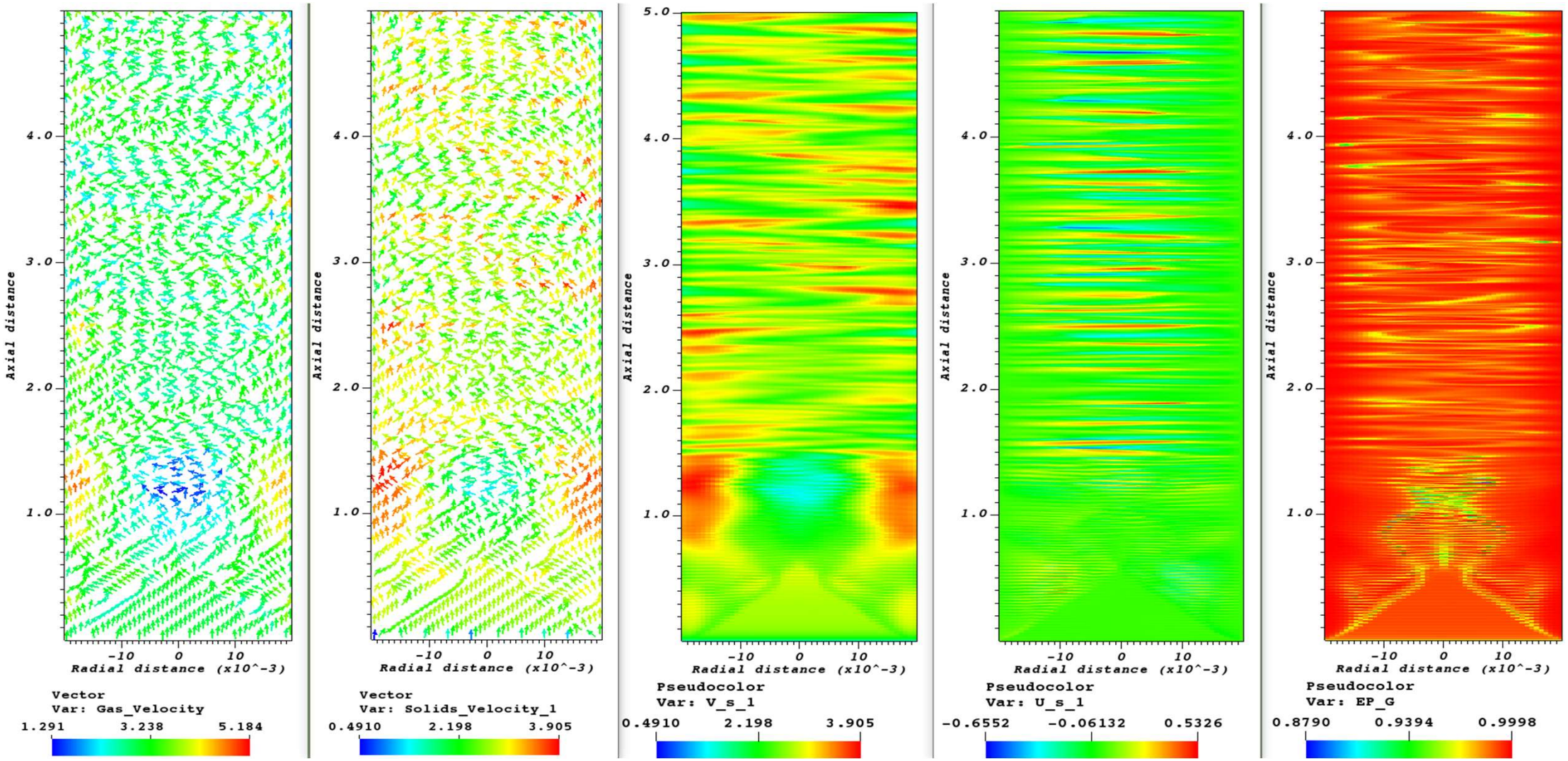

2D Cartesian, grid: 50 x 6250 x 1, $\Delta x \sim 10\ d_p$, $\Delta t \leq$ 1.0E-5, diameter = 0.04 m, height = 5 m, Simonin + Srivastava, Superbee, Gas velocity = 3 m/s, Solids loading = 10, BC_JJ_M, c_e = 0.99, e_w = 0.99, DMP, Preconditioner: 'NONE', (Run urx24rr)
URFAC(1,2,4,9) = 1.0, URFAC((3&5)=0.5, URFAC(8)=0.8

Optimum underrelaxation factors to prevent backflow

- With 2D cartesian grid, Simonin viscous stress model and Pressure Outflow BC, back flow problem was encountered under gas only flow conditions, with the default underrelaxation factors. Outlet gas velocity and pressure were oscillatory, pressure drop was an order of magnitude higher and there were flow reversals.
- Underrelaxation factors are applied to rapidly changing field variables during iterations for stability of calculations. (Syamlal, 1998)
- Results of a statistical experiment with the underrelaxation factors for gas pressure (UR_FAC(1)), V-momentums (UR_FAC(4)) and k-e (UR_FAC(9)) indicated that it is optimum to set all these factors at 1.0 for no/low solids flows. V-momentum (UR_FAC(4)) is the most dominant factor (Rank 1), and it is intuitive: if the axial momentum is throttled relative to the other factors, backflow may occur!
- Considering the profound impact of underrelaxation factors on wall time and stability (measured as the number of stalls/divergences during a simulation), further statistical experiments were carried out to find the optimum values for other factors too.
- Not clear if optimizing underrelaxation factors would prevent backflow for all projects. Some researchers have adjusted the geometry to prevent back flow: Cloete et al. (2013) have used a porous zone at the top; Sabatier et al. (2020) have used a convergent head at the outlet to accelerate the suspension. These measures may increase the computational cost and introduce exit effects.

Note: Default Numerics were used for the simulations carried out for the statistical experiments except for Superbee discretization.

L9 - Taguchi – 3 factors x 3 Levels			Simulation Results		
Gas pressure	V-Momentums	k-e	Range of Vg	Wall time	Pressure drop
UR_FAC(1)	UR_FAC(4)	UR_FAC(9)	m/s	Hrs	Pa
0.5	0.5	0.5	1.33	8.36	-105
0.5	0.8	0.8	0.12	4.52	75
0.5	1.0	1.0	0.06	3.36	65
0.8	0.5	0.8	1.95	5.25	-135 / 415
0.8	0.8	1.0	0.06	3.17	65
0.8	1.0	0.5	0.06	5.16	65
1.0	0.5	1.0	0.15	3.31	65
1.0	0.8	0.5	0.16	5.46	65
1.0	1.0	0.8	0.06	3.78	65

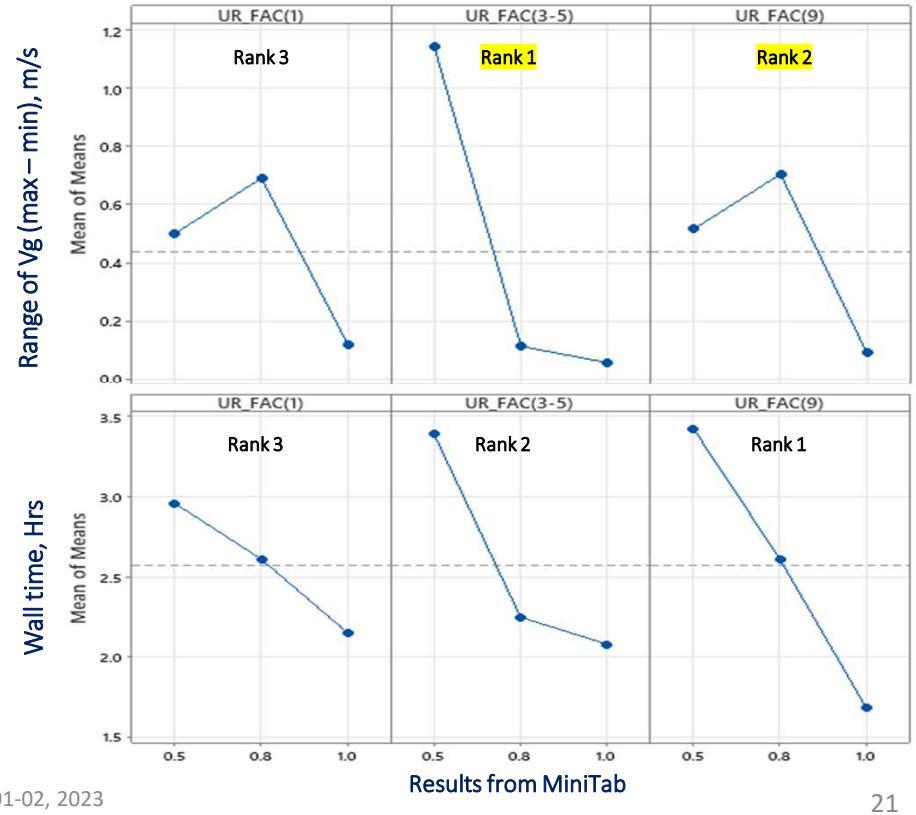

Optimum underrelaxation factors for 2D Cartesian grid simulations #				
Under relaxation factor		Default	Selected	Remarks
UR_FAC(1)	Gas pressure	0.8	0.8	Improves stability
UR_FAC(2)	EP_s	0.5	1.0	
UR_FAC(3&5)	U&W-Momentums	0.5	0.5	Improves stability
UR_FAC(4)	V-Momentums	0.5	1.0	Set at 1.0 to avoid backflow at no / low solids loadings
UR_FAC(8)	Granular temperature	0.5	0.5	~ 1 in 3 runs diverges without underrelaxation
UR_FAC(9)	k-e	0.8	1.0	Set at 1.0 to avoid backflow at no / low solids loadings
UR_F_GS	Drag	1.0	0.0	Improves stability at ~ 3% increase in wall time

- May not be suitable for other coordinate systems or simulation conditions

Simulation results

Core-Annular flow in Cartesian 2D

Results at 5 s, Gas velocity = 3 m/s, Solids loading = 200

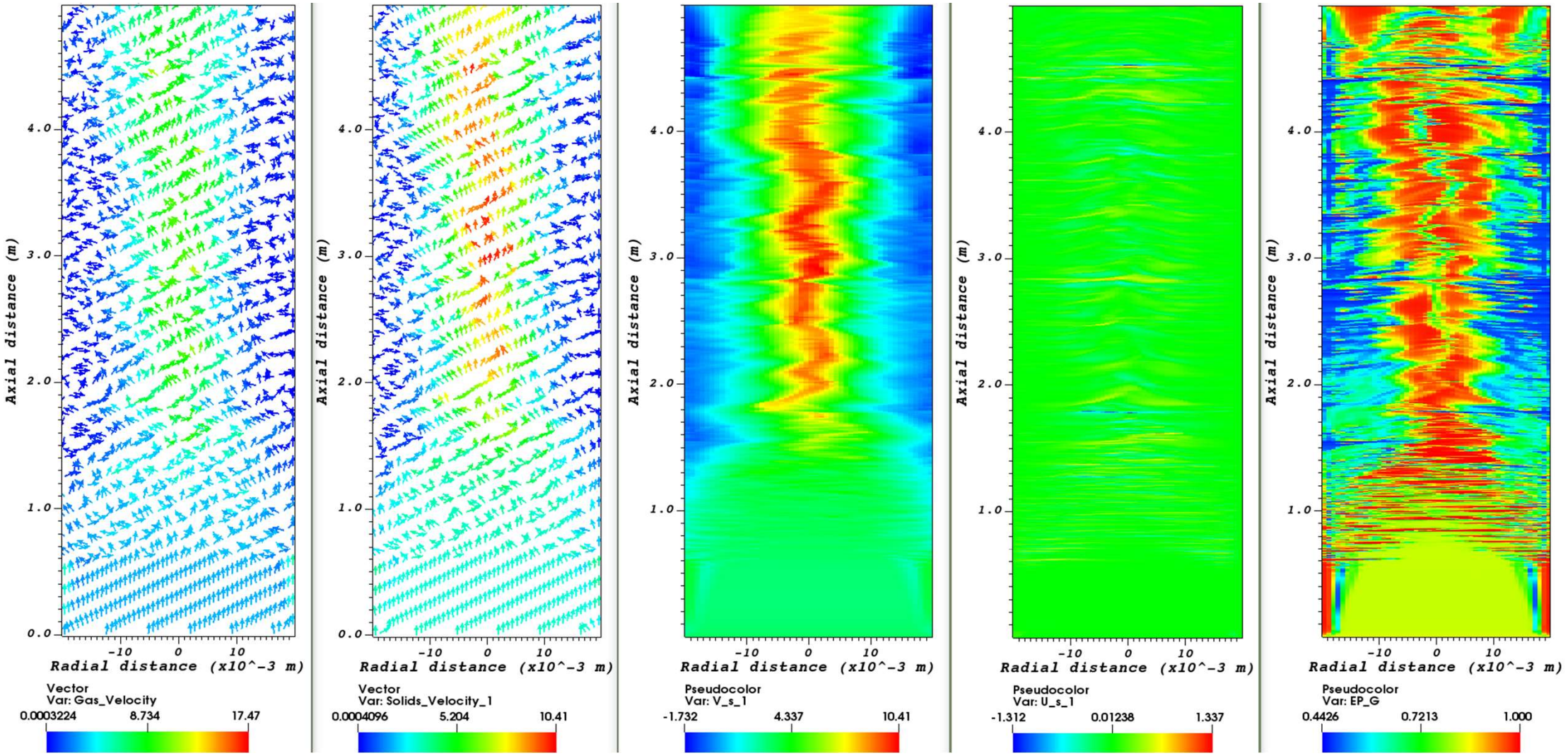

2D Cartesian, grid: 50 x 6250 x 1, $\Delta x \sim 10\ d_p$, $\Delta t \leq$ 1.0E-5 s, diameter = 0.04 m, height = 5 m, Simonin + Srivastava, Superbee, Gas velocity = 3 m/s, Solids loading = 200, BC_JJ_M, c_e = 0.99, e_w = 0.99, DMP, Preconditioner: 'NONE', (Run urx28)

Moving bed flow in cartesian cut-cell

Feed Zone (*F*), Pressure = 3 bar

Results at 5 s, Gas velocity = 3 m/s, Solids loading = 166

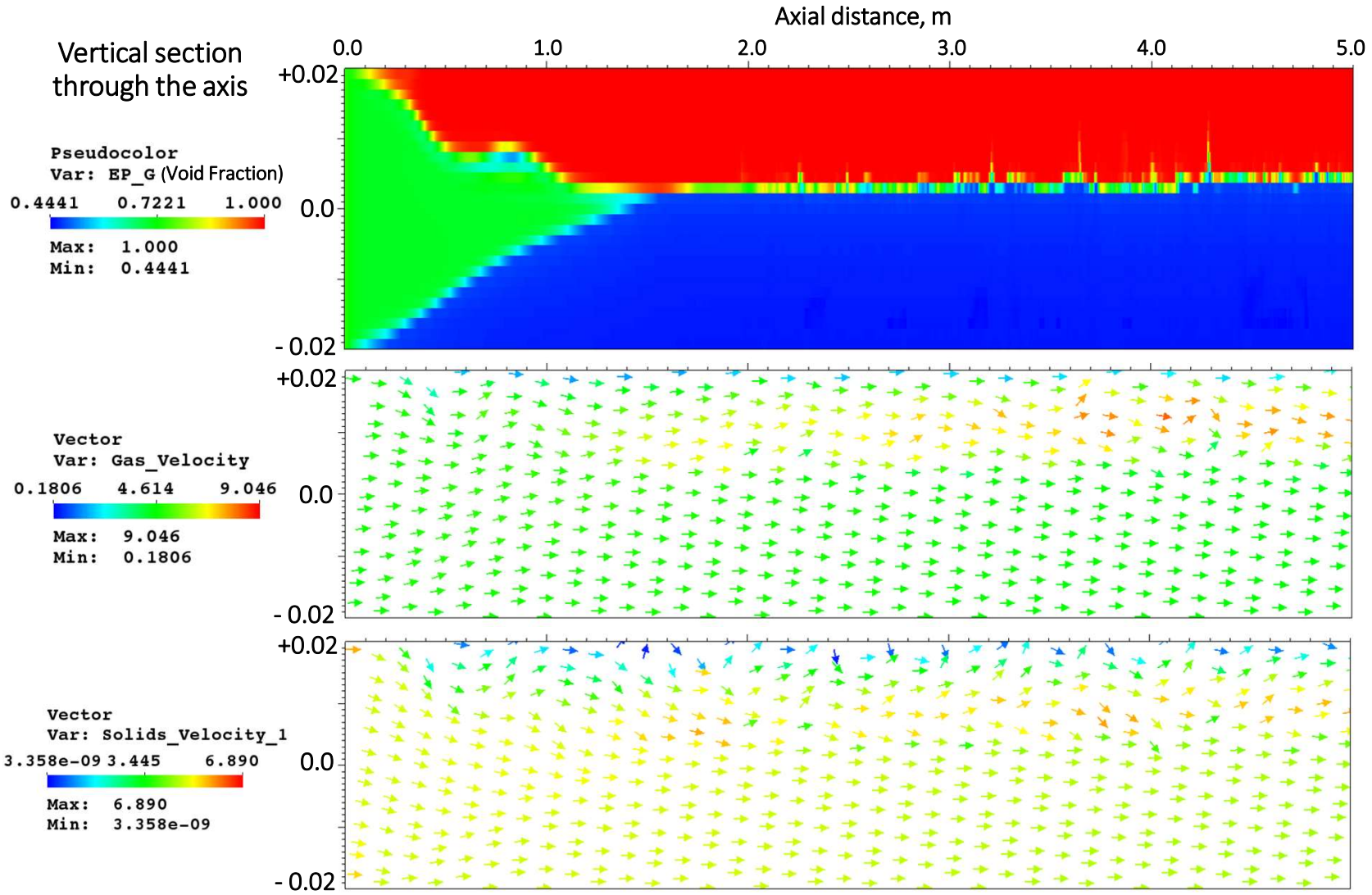

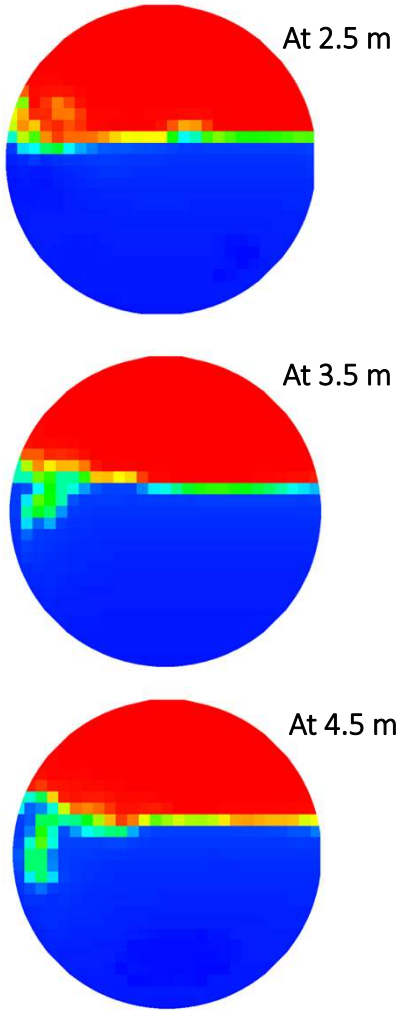

Grid: 27x3375x27, $\Delta x \sim 21\ d_p$, $\Delta t \leq$ 1.0E-4 s, diameter = 0.04 m, length = 5 m, Simonin + Srivastava, Superbee, Gas velocity = 3 m/s, Solids loading = 166, MI-PO, Free slip wall, c_e = 0.87, DMP, Preconditioner: 'NONE', (Run Hori_10)

Moving bed flow in cartesian cut-cell

Ambient receiver (*A*)

Results at 5 s, Gas velocity = 10 m/s, Solids loading = 166

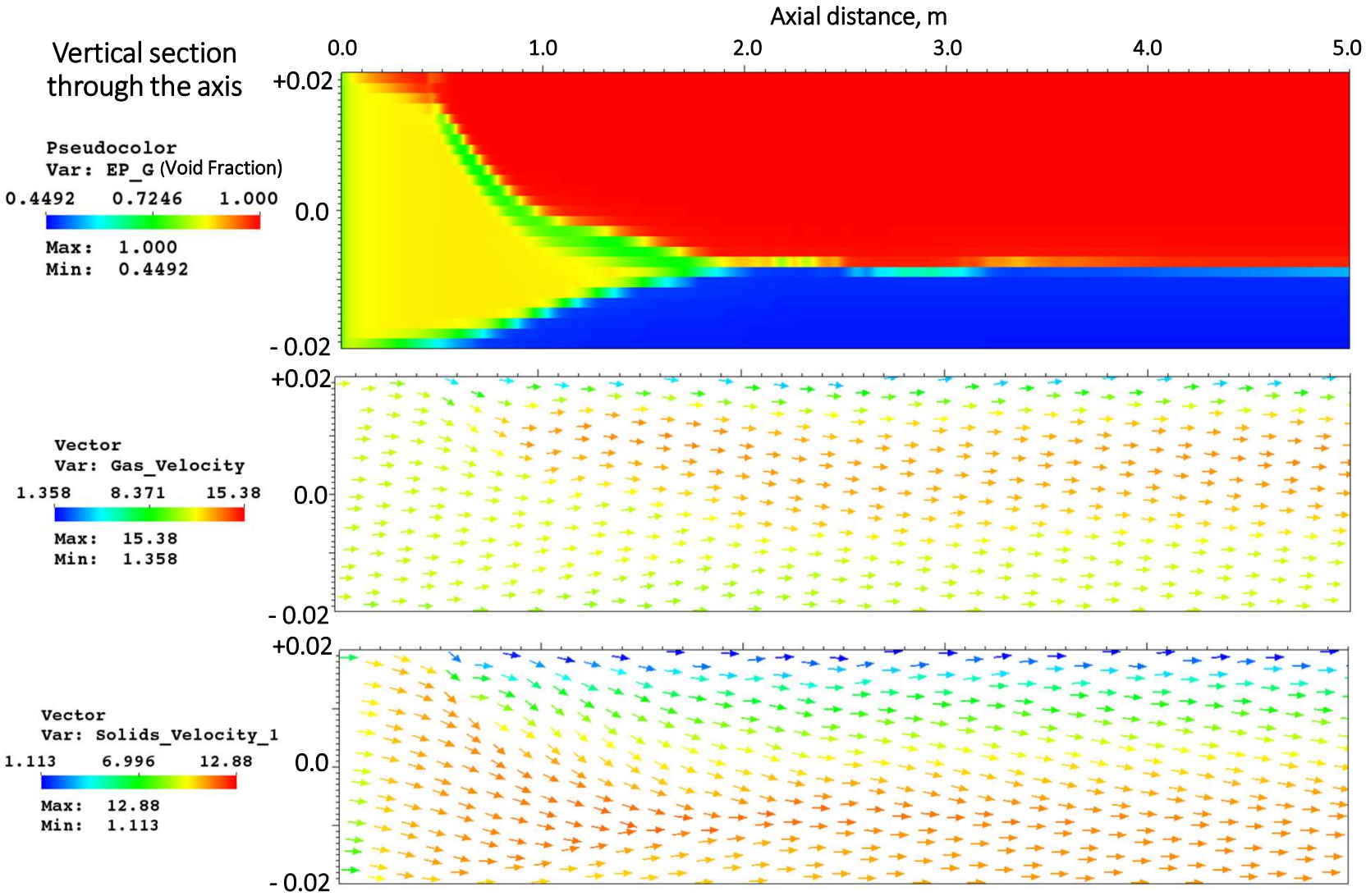

Cross-sectional views

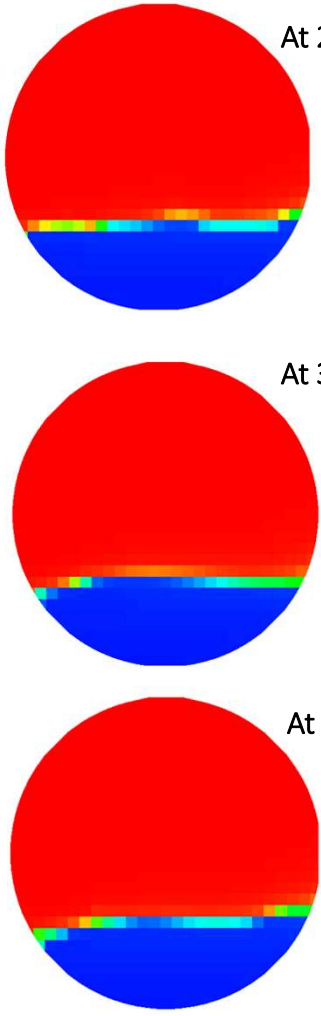

Grid: 27x3375x27, $\Delta x \sim 21\ d_p$, $\Delta t \leq$ 1.0E-4 s, diameter = 0.04 m, length = 5 m, Simonin + Srivastava, Superbee, Gas velocity = 10 m/s, Solids loading = 166, MI-PO, Free slip wall, c_e = 0.87, DMP, Preconditioner: 'NONE', (Run Hori_9)

Conclusions

- **Fluidized dense phase conveying of fine powders situated on the vertical flow phase map of Wirth (1988) and the horizontal flow phase map of Zenz(1949), with inputs from other cited references.**

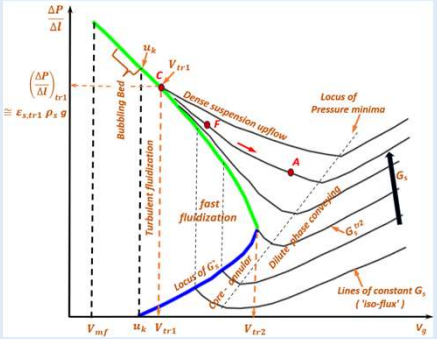

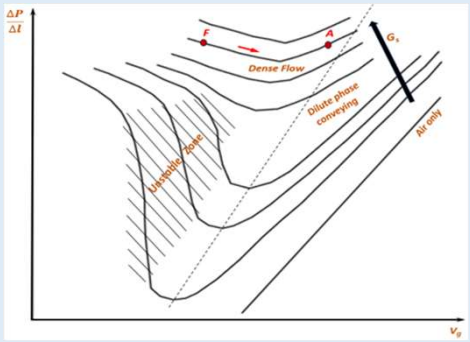

- **Suitability of the Di Felice (1994) drag model (based on the Dalla Valle isolated sphere drag correlation) to cover the full spectrum of solids volume fractions illustrated.**

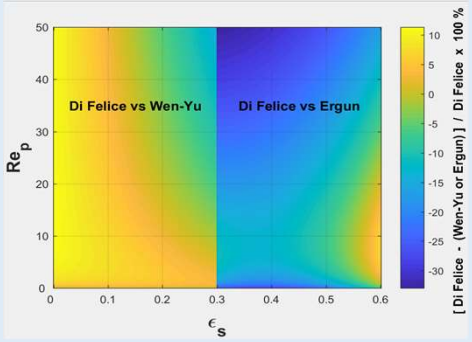

- **Numerical artifacts encountered with 3D cylindrical, cartesian cut-cell and cartesian 2D coordinates highlighted.**
- **Optimum underrelaxation factors for V-momentums and k-e, to avoid backflow with pressure outlet BC proposed.**
- **Ongoing work: To generate rigorous data on spatiotemporal distributions of key parameters (such as solids volume fraction, gas and solids velocities and gas phase pressure) for horizontal and vertical fluidized dense phase conveying with MFiX-TFM.**

Wish list for MFiX-TFM features

- **Johnson & Jackson (1987) partial slip wall BC for Cartesian cut-cell coordinates**
- **Slip-shear (lift) force model**
- **Cohesion model for mildly cohesive powders such as the Gu et al.(2019)**
- **Option to specify fully developed flow profile at the inlet BC to minimize the inlet transition length.**

References

Agrawal, K. *et al.* (2001) 'The role of meso-scale structures in rapid gas-solids flows', *Journal of Fluid Mechanics*, 445, pp. 151–185.

Arastoopour, H., Gidaspow, D. and Abbasi, E. (2017) *Computational Transport Phenomena of Fluid-Particle Systems*. Cham: Springer. Available at: https://doi.org/10.1007/978-3-319-45490-0.

Askarishahi, M., Salehi, M. and Radl, S. (2022) 'Capability of the TFM Approach to Predict Fluidization of Cohesive Powders', *Industrial & Engineering Chemistry Research*, 61. Available at: https://doi.org/10.1021/acs.iecr.1c04786.

Avidan, A.A. and Yerushalmi, J. (1982) 'Bed expansion in high velocity fluidization', *Powder technology*, 32(2), pp. 223–232.

Bakshi, A. *et al.* (2015) 'Eulerian-Eulerian simulation of dense solid-gas cylindrical fluidized beds: Impact of wall boundary condition and drag model on fluidization', *Powder Technology*, 277, pp. 47–62. Available at: https://doi.org/10.1016/j.powtec.2015.02.056.

Bakshi, A., Altantzis, C. and Ghoniem, A.F. (2014) 'Towards accurate three-dimensional simulation of dense multi-phase flows using cylindrical coordinates', *Powder Technology*, 264, pp. 242–255.

Balzer, G. *et al.* (1996) 'A unifying modelling approach for the numerical prediction of dilute and dense gas–solid two phase flow', in *CFB5, 5th Int. Conf. on Circulating Fluidized Beds*. Beijing, China.

Beetstra, R., van der Hoef, M.A. and Kuipers, J.A.M. (2007) 'Drag Force of Intermediate Reynolds Number Flow Past Mono- and Bidisperse Arrays of Spheres', *AIChE Journal*, 53(2), pp. 489–501. Available at: https://doi.org/10.1002/aic.11065.

Benyahia, S. (2012) 'Fine-Grid Simulations of Gas-Solids Flow in a Circulating Fluidized Bed', *AIChE Journal*, 58(11), pp. 3589–3592. Available at: https://doi.org/10.1002/aic.13826.

Benyahia, S., Syamlal, M. and O'Brien, T.J. (2005) 'Evaluation of boundary conditions used to model dilute , turbulent gas / solids flows in a pipe', *Powder Technology*, 156, pp. 62–72. Available at: https://doi.org/10.1016/j.powtec.2005.04.002.

Benyahia, S., Syamlal, M. and O'Brien, T.J. (2007) 'Study of the ability of multiphase continuum models to predict core-annulus flow', *AIChE Journal*, 53(10), pp. 2549–2568. Available at: https://doi.org/10.1002/aic.11276.

Breault, R.W. (2023) 'Scaling CFB risers: Maintaining microstructure dynamics', *Powder Technology*, 415(118191).

Breault, R.W. and Weber, J. (2021) 'Saturation Carrying Capacity for Group A Particles in a Circulating Fluidized Bed', *Energies (Basel)*, 14(10), pp. 2809-.

Cloete, S., Johansen, S.T. and Amini, S. (2013) 'Investigation into the effect of simulating a 3D cylindrical fluidized bed reactor on a 2D plane', *Powder technology*, 239, pp. 21–35.

Cocco, R., Karri, R.S.B. and Knowlton, T. (2010) '10. Circulating Fluidized Beds', in *Computational Gas-Solids Flows and Reacting Systems. Editors: Pannala S, Syamlal M, O'Brien TJ*. Hershey: IGI Global.

Di Felice, R. (1994) 'The voidage function for fluid-particle interaction systems', *International journal of multiphase flow*, 20(1), pp. 153–159.

Drake, T.G. (1991) 'Granular flow: physical experiments and their implications for microstructural theories', *Journal of Fluid Mechanics*, 225, pp. 121–152.

Fede, P., Simonin, O. and Ingram, A. (2016) '3D numerical simulation of a lab-scale pressurized dense fluidized bed focussing on the effect of the particle-particle restitution coefficient and particle-wall boundary conditions', *Chemical Engineering Science*, 142, pp. 215–235. Available at: https://doi.org/10.1016/j.ces.2015.11.016.

Foerster, S.F. *et al.* (1994) 'Measurements of the collision properties of small spheres', *Physics of Fluids*, 6(3). Available at: https://doi.org/10.1063/1.868282.

Gobin, A. *et al.* (2003) 'Fluid dynamic numerical simulation of a gas phase polymerization reactor', *International Journal for Numerical Methods in Fluids*, 43, pp. 1199–1220.

Grace, J.R. (2000) 'Reflections on turbulent fluidization and dense suspension upflow', *Powder Technology*, 113(3), pp. 242–248. Available at: https://doi.org/10.1016/S0032-5910(00)00307-7.

Gu, Y. *et al.* (2019) 'Computationally generated constitutive models for particle phase rheology in gas-fluidized suspensions', *Journal of Fluid Mechanics*, 860, pp. 318–349. Available at: https://doi.org/10.1017/jfm.2018.856.

Hill, R.J., Koch, Donald L and Ladd, A.J.C. (2001) 'Moderate-Reynolds-number flows in ordered and random arrays of spheres', *Journal of fluid mechanics*, 448, pp. 243–278.

Hill, R.J., Koch, DONALD L. and Ladd, A.J.C. (2001) 'The first effects of fluid inertia on flows in ordered and random arrays of spheres', *Journal of fluid mechanics*, 448, pp. 213–241.

Issangya, A.S. *et al.* (2023) 'Solids flux profiles of Geldart Group A particles in high-velocity circulating fluidized bed risers', *The Canadian Journal of Chemical Engineering*, 101(1), pp. 256–268. Available at: https://doi.org/10.1002/cjce.24628.

Johnson, P.C. and Jackson, R. (1987) 'Frictional-collisional constitutive relations for granular materials , with application to plane shearing', *Journal of Fluid Mechanics*, 176, pp. 67–93.

Kandhai, D., Derksen, J.J. and Van den Akker, H.E.A. (2003) 'Interphase drag coefficients in gas-solid flows', *AIChE journal*, 49(4), pp. 1060–1065.

Kim, S.W. *et al.* (2004) 'Flow behavior and regime transition in a high-density circulating fluidized bed riser', *Chemical engineering science*, 59(18), pp. 3955–3963.

References

Kirkpatrick, M.P., Armfield, S.W. and Kent, J.H. (2003) 'A representation of curved boundaries for the solution of the Navier–Stokes equations on a staggered three-dimensional Cartesian grid', *Journal of Computational Physics*, (184), pp. 1–36.

Klinzing, G.E. *et al.* (2010) *Pneumatic Conveying of Solids A theoretical and practical approach*. 3rd edn. Dordrecht: Springer.

Kunii, D. and Levenspiel, O. (1991) *Fluidization Engineering*. 2nd edn. Butterworth-Heinemann.

Lathouwers, D. and Bellan, J. (2000) 'Modeling of dense gas-solid reactive mixtures applied to biomass pyrolysis in a fuidized bed', in *Proceedings of the 2000 U.S. DOE Hydrogen Program Review*.

Li, T. *et al.* (2014) 'CFD simulations of circulating fluidized bed risers, part I: Grid study', *Powder Technology*, 265(C), pp. 2–12. Available at: https://doi.org/10.1016/j.powtec.2014.04.008.

Li, T. and Benyahia, S. (2012) 'Revisiting Johnson and Jackson Boundary Conditions for Granular Flows', *AIChE Journal*, 58(7), pp. 2058–2068. Available at: https://doi.org/10.1002/aic.

Li, T., Pannala, S. and Shahnam, M. (2014) 'CFD simulations of circulating fluidized bed risers, part II, evaluation of differences between 2D and 3D simulations', *Powder Technology*, 254, pp. 115–124. Available at: https://doi.org/10.1016/j.powtec.2014.04.007.

Loezos, P.N., Costamagna, P. and Sundaresan, S. (2002) 'The role of contact stresses and wall friction on fluidization', *Chemical Engineering Science*, 57(24), pp. 5123–5141. Available at: https://doi.org/10.1016/S0009-2509(02)00421-9.

Lu, B., Wang, W. and Li, J. (2009) 'Searching for a mesh-independent sub-grid model for CFD simulation of gas–solid riser flows', *Chemical engineering science*, 64(15), pp. 3437–3447.

Massoudi, M. (2003) 'Constitutive relations for the interaction force in multicomponent particulate flows', *International journal of non-linear mechanics*, 38(3), pp. 313–336.

Mckeen, T. and Pugsley, T. (2003) 'Simulation and experimental validation of a freely bubbling bed of FCC catalyst', *Powder Technology*, 129, pp. 139–152.

Mills, D. (2004) *Pneumatic conveying design guide*. 2nd edn. Amsterdam: Elsevier, Butterworth Heinemann.

Monazam, E.R. and Shadle, L.J. (2011) 'Method and Prediction of Transition Velocities in a Circulating Fluidized Bed's Riser', *Industrial & Engineering Chemistry Research*, 50(4), pp. 1921–1927. Available at: https://doi.org/10.1021/ie1013376.

Patro, P. and Dash, S.K. (2014) 'Numerical simulation for hydrodynamic analysis and pressure drop prediction in horizontal gas-solid flows', *Particulate Science and Technology*, 32(1), pp. 94–103. Available at: https://doi.org/10.1080/02726351.2013.829543.

Sabatier, F. *et al.* (2020) 'Experiments support simulations by the NEPTUNE_CFD code in an Upflow Bubbling Fluidized Bed reactor', *Chemical engineering journal (Lausanne, Switzerland : 1996)*, 385, pp. 123568-.

Srivastava, A. and Sundaresan, S. (2003) 'Analysis of a frictional – kinetic model for gas – particle flow', *Powder Technology*, 129, pp. 72–85. Available at: https://doi.org/10.1016/S0032-5910(02)00132-8.

Syamlal, M. (1998) *MFIX Documentation Numerical Technique*. January. Morgantown: U.S. Department of Energy, Federal Energy Technology Center, p. DE-AC21-95MC31346.

Syamlal, M., Celik, I.B. and Benyahia, S. (2017) 'Quantifying the uncertainty introduced by discretization and time-averaging in two-fluid model predictions', *AIChE Journal*, 63(12), pp. 5343–5360. Available at: https://doi.org/10.1002/aic.15868.

Syamlal, M. and O'Brien, T. (1987) 'The derivation of a drag coefficient formula from velocity-voidage correlations', *Technical Note, US Department of energy, Office of Fossil Energy, NETL, Morgantown, WV* [Preprint].

Tang, Y. *et al.* (2015) 'A New Drag Correlation from Fully Resolved Simulations of Flow Past Monodisperse Static Arrays of Spheres', *AIChE Journal*, 61(2), pp. 688–698. Available at: https://doi.org/10.1002/aic.14645.

Tenneti, S., Garg, R. and Subramaniam, S. (2011) 'Drag law for monodisperse gas–solid systems using particle-resolved direct numerical simulation of flow past fixed assemblies of spheres', *International journal of multiphase flow*, 37(9), pp. 1072–1092.

Wang, C. *et al.* (2022) 'Flow characteristics in a pilot-scale circulating fluidized bed with high solids flux up to 1800 kg/m2 s', *Powder Technology*, 405, p. 117542. Available at: https://doi.org/10.1016/j.powtec.2022.117542.

Wang, J., van der Hoef, M.A. and Kuipers, J.A.M. (2011) 'The role of scale resolution versus inter-particle cohesive forces in two-fluid modeling of bubbling fluidization of Geldart A particles', *Chemical Engineering Science*, 66(18), pp. 4229–4240. Available at: https://doi.org/10.1016/j.ces.2011.06.004.

Wirth, K.-E. (1988) 'Axial pressure profile in Circulating Fluidized Beds', *Chemical Engineering and Technology*, 11(1), pp. 11–17.

Yang, W.-C. (2007) 'Modification and re-interpretation of Geldart's classification of powders', *Powder Technology*, 171(2), pp. 69–74. Available at: https://doi.org/10.1016/j.powtec.2006.08.024.

Yerushalmi, J. and Avidan, A. (1985) 'Chapter 7. High-Velocity Fluidization', in J.F. Davidson, R. Clift, and D. Harrison (eds) *Fluidization*. 2nd edn. United States: Academic Press, Inc.,Orlando, FL.

Thank you!

I acknowledge the support received at the MFiX forum.

Please forward your comments to prabu.balasubramanian@gcu.ac.uk